NEAR-INFRARED DUAL BIOLUMINESCENCE IMAGING IN MOUSE MODELS OF CANCER USING INFRALUCIFERIN

Cassandra L. Stowe [1,2], Thomas A. Burley [3], Helen Allan [4], Maria Vinci [3], Gabriela Kramer-Marek [3], Daniela M. Ciobota [3], Gary N. Parkinson [5], Tara L. Southworth [6], Giulia Agliardi [1], Alastair Hotblack [1], Mark F. Lythgoe [2], Bruce R. Branchini [6], Tammy L. Kalber [2], James C. Anderson [4*], Martin A. Pule [1*]

[1] University College London, Cancer Institute, 72 Huntley Street, London, WC1E 6DD, United Kingdom

[2] University College London, Centre for Advanced Biomedical Imaging, 72 Huntley Street, London, WC1E 6DD, United Kingdom

[3] The Institute of Cancer Research, 123 Old Brompton Road, London, SW7 3RP, UK, United Kingdom

[4] University College London, Department of Chemistry, 20 Gordon Street, London, WC1H 0AJ, United Kingdom

[5] University College London, School of Pharmacy, 29-39 Brunswick Square, Bloomsbury, London WC1N 1AX, United Kingdom

[6] Department of Chemistry, Connecticut College, New London, Connecticut, 06320, USA

[*]Correspondence should be addressed to M.A.P. (martin.pule@ucl.ac.uk) or J.C.A. (j.c.anderson@ucl.ac.uk)

ABSTRACT

Bioluminescence imaging (BLI) is ubiquitous in scientific research for the sensitive tracking of biological processes in small animal models. However, due to the attenuation of visible light by tissue, and the limited set of near-infrared bioluminescent enzymes, BLI is largely restricted to monitoring single processes *in vivo*. Here we show, that by combining stabilised colour mutants of firefly luciferase (FLuc) with the luciferin (LH_2) analogue infraluciferin (iLH_2), near-infrared dual BLI can be achieved*in vivo*. The X-ray crystal structure of FLuc with a high-energy intermediate analogue, 5'-O-[N-(dehydroinfraluciferyl)sulfamoyl] adenosine (iDLSA) provides insight into the FLuc-iLH_2 reaction leading to near-infrared light emission. The spectral characterisation and unmixing validation studies reported here established that iLH_2 is superior to LH_2 for the spectral unmixing of bioluminescent signals *in vivo*; which led to this novel near-infrared dual BLI system being applied to monitor both tumour burden and CAR T cell therapy within a systemically induced mouse tumour model.

INTRODUCTION

Bioluminescence imaging (BLI) is used extensively for the sensitive, longitudinal and high-throughput monitoring of biological processes *in vivo* [1,2,3,4,5]. Bioluminescence light emission is produced through the catalysis of a small molecule substrate, most commonly D-luciferin (D-LH_2), by a luciferase enzyme. The mutagenesis of bioluminescent enzymes has improved the sensitivity and accuracy of BLI in small animals [6,7]. However, despite its widespread use in scientific research, BLI is still largely restricted to tracking a single parameter *in vivo*. The ability to discretely monitor two biological parameters (dual-BLI) simultaneously within a single animal is highly desirable [1] with potential uses ranging from the monitoring of tumour burden alongside cellular therapy, to the visualisation of dynamic biological processes such as protein-protein interactions [8].

Previous approaches to dual-BLI have been disappointing. The use of multiple bioluminescent proteins which catalyse different substrates is the most frequently used method but suffers from a number of limitations. Sequential substrate administration is normally required, in addition this method commonly employs a combination of a coelenterazine and a D-LH_2 utilising luciferase (with the blue emission from the former being heavily absorbed compared to the yellow-green emission from the latter) [9,10]. Differences in biodistribution and reaction kinetics of two substrates can make image co-registration and interpretation difficult. The development of orthogonal luciferase-luciferin pairs has solved some of these limitations but this approach still requires multiple substrate administrations [11].

An ideal dual-BLI approach would use two spectrally distinct bioluminescent proteins utilising a single substrate followed by spectral unmixing of the signal. However, this approach is not currently feasible using LH_2. Although luciferases can be mutated to alter the

colour of their emission, a limit appears to have been reached for mutational colour modulation of firefly and related luciferases. The most red-shifted of these enzymes have maximal peak emissions between 610 and 620nm [6]. This is insufficient for dual BLI *in vivo*. Due to the differential attenuation of light by biological tissue spectral unmixing of a red-shifted luciferase paired with a standard or green-shifted enzyme is challenging, especially in deeper tissue models [12]. Shifting the emission of both enzymes into the near infrared must be achieved to allow adequate unmixing. To further red-shift peak emission we and others have turned to chemical modification of the D-luciferin (LH_2) substrate [13]. We recently described the LH_2 analogue infraluciferin (iLH_2) which has a luciferase dependent red-shifted peak emission of up to 706nm [14] (**Figure 1a**). We hypothesized that combining colour modulation of bioluminescence through mutagenesis of the FLuc protein along with red-shifting bioluminescence by chemical modification of LH_2 would allow dual-BLI, an approach that has not been described previously.

In this work, we explored the possible structural interactions in the enzyme that may account for the near infrared emission of iLH2 and its application to dual-BLI *in vivo*. First, the X-ray crystal structure of FLuc in complex with a high-energy intermediate analogue, 5'-O-[(N-dehydroinfraluciferyl)-sulfamoyl] adenosine (iDLSA) was determined to provide insight into the FLuc-iLH_2 light-emitting reaction. Next, we selected a pair of stabilized colour-shifted FLuc mutants, which emit with a 20nm separation in peak emission wavelength with iLH_2 in the near infrared. We demonstrated the ability to spectrally unmix these two biological signals *in vivo* at depth using iLH_2. Finally, we show a proof-of-concept of utility using this novel dual imaging technique to longitudinally monitor both tumour burden and chimeric antigen receptor (CAR) T cell therapy within a single animal model.

RESULTS

Crystal structure of firefly luciferase in complex with a iLH_2 analogue

To help understand the red shift in bioluminescence emission from FLuc that is observed in its reaction with iLH_2, the X-ray crystal structure of FLuc in complex with iDLSA was resolved and is shown in **Figure 1b** (PDB ID: 6HPS). Data collection and refinement statistics (molecular replacement); and data collection, phasing and refinement statistics for mad (semet) structures can be found in **Figure 1 -Figure supplement 1**. iDLSA captures FLuc in the adenylation step of the light emitting reaction (^{1}H and ^{13}C data spectra synthetic chemical compounds can be found in **Figure 1 – Figure supplement 2**). The conformation of the iLH_2 heterocyclic rings with respect to the alkene, as drawn in **Figure 1a**, is confirmed to be as predicted by computational studies and is the most likely conformation of the light emitting form [15]. This newly crystallised FLuc structure was aligned with the reported structure of FLuc with 5'-O-[(N-dehydroluciferyl)-sulfamoyl] adenosine (DLSA) (PDB ID: 4G36) [16]. The structures show good alignment to each other, however there is evidence of a more open active site supported by a reduction in root-mean-squared (RMSD) score when aligned based on just the N-terminal domain of FLuc rather than the entire structure (RMSD = 0.688 and 0.783 respectively) (**Figure 1c**).

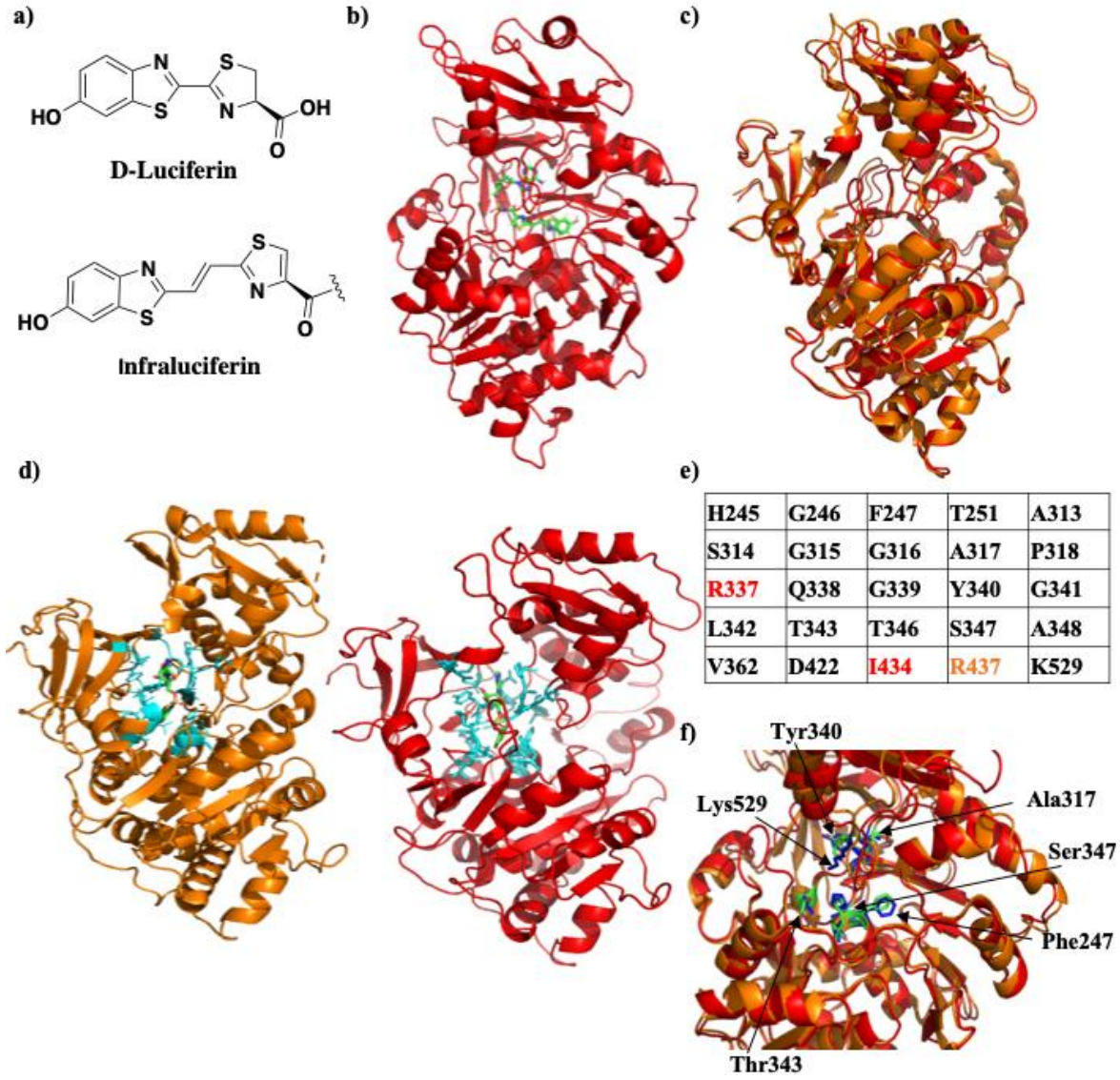

H245	G246	F247	T251	A313
S314	G315	G316	A317	P318
R337	Q338	G339	Y340	G341
L342	T343	T346	S347	A348
V362	D422	I434	R437	K529

Figure 1: Crystal structure of Firefly luciferase in complex with a iLH_2 analogue

a) Chemical structures of native D-Luciferin (LH_2) and the LH_2 analogue infraluciferin (iLH_2).

b) The crystal structure of Firefly luciferase (FLuc) in complex with the infraluciferyl-adenylate analogue 5'-O-[(N-dehydroinfraluciferyl)-sulfamoyl] adenosine (iDLSA) resolved to a 3.2 Å resolution (PDB ID: 6HPS).

c) The structure of FLuc in complex with the iLH_2 analogue iDLSA aligned to the reported structure of FLuc in complex with the LH_2 analogue 5'-O-[(N-dehydroluciferyl)-sulfamoyl] adenosine (DLSA) (PDB ID: 4G36) [16] based on the FLuc N-terminal domain (residues 1-436). The structure of FLuc in complex with iLH_2 is shown in red, and the structure of FLuc in complex with LH_2 is shown in orange.

d) The structure of FLuc in complex with luciferin analogue DLSA (PDB ID: 4G36) (orange) and the infra-luciferin analogue iDLSA (red). Those residues within 4 Å of the substrate in each structure are highlighted in blue.

e) The table lists all residues within 4 Å of the both substrates, with those in orange or red only being found within 4 Å of DLSA and iDLSA respectively.

f) Highlights the same 7 active site residues for both the aligned structures, with FLuc iLH_2 residues in blue and FLuc LH_2 residues in green.

All analysis performed in PyMOL software (Schrodinger).

Figure 1 - Figure supplement 1 *provides data tables for data collection and refinement statistics (molecular replacement); and data collection, phasing and refinement statistics for mad (semet) structures*.
Figure 1 - Figure supplement 2 *provides ^{1}H and ^{13}C data for synthetic chemical compounds.*

All FLuc residues in close proximity (4 Å) to DLSA were also found to be within the same distance to iDLSA, with the exception of Arg437, > 4 Å away from iDLSA (**Figure 1d and e**). We noted that despite differences in the conformation of iDLSA compared to DLSA in both 4G36 and *L. cruciata* 2D1S [17] structures, the positions of the phenolic groups are quite similar (~0.5 Å). The altered position of the benzothiazole ring and the greater size of iDLSA may be the cause of a series of small active site changes that affect residues Glu311, Arg337, Asn338, Gly339, and Thr343 resulting in a total of 6 differences in H-bonding interactions. When specific residues implicated in the light emitting reaction [16] were measured between the two structures differences ranged from 0.7 – 1.6 Å; with the biggest divergence being Lys529 (found in the C-terminal cap) which had a 2.4 Å difference in the nitrogen residue found in the side chain of the amino acid (**Figure 1f**). The resulting increase in active site polarity due to the rotation of the C-terminal cap, if maintained during the light emitting conformation, could contribute to the red-shift in light emission [17], in addition to the increased π-conjugation through the chemical structure of the emitter. This X-ray structure will help the future design of more efficient FLuc-iLH_2 pairs.

Spectral unmixing of firefly luciferase mutants in vitro

A range of colour-shifted, thermo- and pH stable FLuc mutants were spectrally characterised *in vitro* with a comparative selection of LH_2 analogues proven to red-shift bioluminescence emission (CycLuc1[18], Aka-Lumine-HCL[19] and iLH_2 [14]). Two new luciferins NH_2-$NpLH_2$ and OH- $NpLH_2$ have also been shown to have near infrared emissions [20] but these were reported too late to include in this study. FLuc mutants were engineered to combine mutations

reported to provide superior stability [21] and colour-shifting capability [22] (stabilising and colour shifting FLuc mutations are detailed in ***materials and methods)***. The Raji B lymphoma cell line engineered to express a FLuc mutant were spectrally imaged after addition of each substrate. These cell lines were subsequently used for all *in vitro* and *in vivo* testing. Both CycLuc1 and Aka-Lumine-HCL showed a consistent red-shift in peak bioluminescence emission wavelength to ~600nm and ~660nm respectively for all FLuc mutants, making these substrates unsuitable for dual colour BLI (**Figure 2 – Figure supplement 1**). The data confirmed that with LH_2 both FLuc_natural and FLuc_green have a peak emission of ~560nm, whilst FLuc_red has a peak emission of ~620nm (**Figure 2 – Figure supplement 1**) [21, 22]. When tested with iLH_2 all FLuc mutants were shifted >100nm into the near infrared but maintained their relative spectral shift [FLuc_green ~680nm, FLuc_natural ~700nm and FLuc_red ~720nm (**Figure 2 – Figure supplement 1**)]. From this we progressed further with two FLuc mutants, FLuc_green and FLuc_red to explore their utility for dual-BLI.

The ability to spectrally unmix FLuc_green and FLuc_red (**Figure 2a**) *in vitro* was investigated by mixing the two FLuc_mutants expressed in the Raji B lymphoma cell line at various ratios followed by spectral imaging and unmixing with both LH_2 and iLH_2 (**Figure 2b)**. As would be expected from accurate spectral unmixing, the top wells were classified as containing mostly FLuc_green signal, which gradually decreased down the plate in line with the decreasing proportions of FLuc_green expressing cells, with the bottom wells being largely classified as FLuc_red signal for both LH_2 and iLH_2. The percentage unmixed signal of FLuc_green and FLuc_red was plotted for each ratio of FLuc expressing cells (**Figure 2c**). Correlation analysis was performed on this data comparing input cellular proportions with unmixed signal, giving R^2 values of 0.9983 and 0.9972 for LH_2 and iLH_2 respectively. Even

though all 18 bandpass filters equipped on the IVIS Spectrum were utilised for spectral unmixing in this *in vitro* testing, we appreciate that not all potential users of this novel dual bioluminescence methodology will have access to machines with such a wide selection of bandpass filters. Therefore, further analysis of our data showed that spectral unmixing could be achieved with high accuracy just using a subset of filters. For LH_2, the use of 3 bandpass filters (500, 660nm, 820nm) gave an R^2 value of 0.9958; For iLH_2, the use of 3 bandpass filters (600nm, 700nm, 800nm) gave an R^2 value of 0.9937. The highest accuracy of spectral unmixing we could achieve using just 2 filters were R^2 values of 0.9776 and 0.9775 for LH_2 (500nm and 720nm) and iLH_2 (600nm and 720nm) respectively. Additionally, an experiment was carried out where FLuc_green and FLuc_red have been expressed at different levels in the same cell. Spectral bioluminescence imaging and unmixing has subsequently been performed to successfully reflect these differing expression levels with both LH_2 and iLH_2 (**Figure 2 – Figure supplement 2**). This spectral imaging data shows that both LH_2 and iLH_2 can be used for dual bioluminescence reporting *in vitro*.

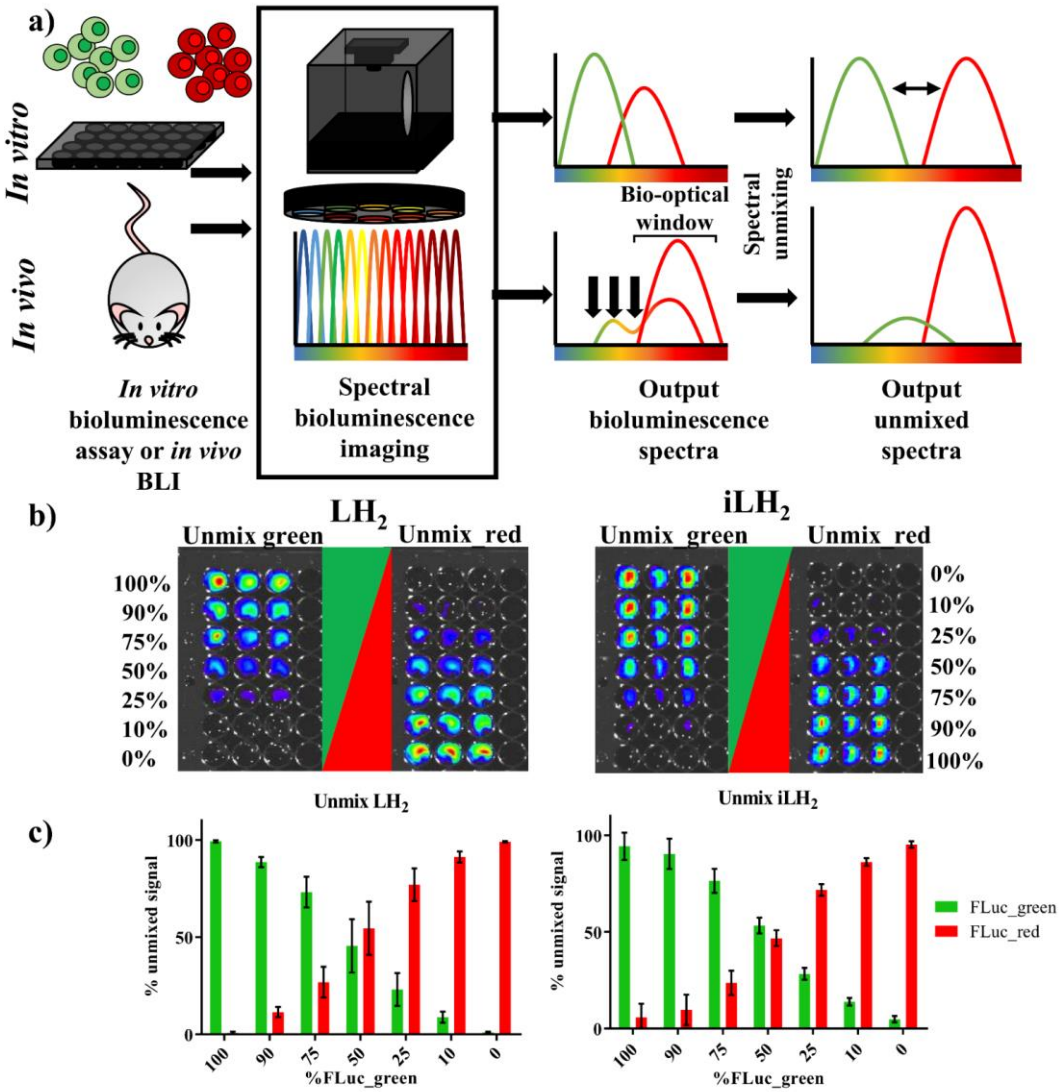

Figure 2: Spectral unmixing of Firefly luciferase mutants in vitro

(a) Bioluminescence spectral unmixing of cells expressing colour-shifted Firefly luciferase (FLuc) mutants, for both in vitro assays and in vivo animal models, requires spectral bioluminescence imaging through a series of bandpass filters. Bioluminescence spectral imaging acquires spectral data, which can then be deconvoluted into its separate components. As depicted, spectral unmixing in vivo is significantly more challenging due to attenuation of bioluminescent signal that does not fall within the bio-optical window.

(b) FLuc colour mutants FLuc_green and FLuc_red expressed in the B lymphoma Raji cell line were mixed in various proportions (0-100% of the total population). After addition of either D-luciferin (LH_2) or infraluciferin (iLH_2) plates were spectrally imaged using the IVIS Spectrum (Perkin Elmer).Unmixed green and unmixed red output images produced from library spectral unmixing using Living Image software (Perkin Elmer) for both substrates.

(c) Percentage unmixed signal of FLuc_green and FLuc_red for each ratio of FLuc expressing cells tested when imaged with LH_2 and iLH_2. Signal adjusted to 100% populations. Mean and standard deviation plotted (n=6 for both LH_2 and iLH_2).

Figure 2 – Figure supplement 1 *gives the spectra of x11 FLuc mutants FLuc_natural, FLuc_green and FLuc_red with LH_2 analogues (a) LH_2, b) iLH_2, c) CycLuc1 and d) Aka-Lumine-HCL) in vitro, alongside the chemical structure of CycLuc1 and Aka-Lumine-HCL below the corresponding spectra). Spectra normalised to peak emission for each FLuc mutant with each substrate. Each point on the x-axis gives the midpoint of the 20nm band pass filter used in spectral imaging.*

Figure 2 – Figure supplement 2 *whether FLuc_green and FLuc_red could be successfully spectrally unmixed when expressed in the same cell was also explored. The mammalian B Lymphoma Raji cell line was transduced with FLuc_green and FLuc_red, which was then sorted by flow cytometry using co-expressed marker genes to get cell populations with differing expression levels of the two luciferases enzymes.*

(a) The normalised median fluorescence intensity (MFI) of FLuc_green and FLuc_red for each cellular population

(b) Differing combinations of low and high expression levels of FLuc_green and FLuc_red could be detemined using spectral bioluminescence imaging and spectral unmixing with both LH_2 and iLH_2.

Spectral characterisation of firefly luciferase mutants with LH_2 and iLH_2 in vivo

To investigate the use of FLuc_green and FLuc_red with LH_2 and iLH_2 for *in vivo* dual BLI three NOD *scid* gamma (NSG) tumour models, representing increasing tissue depth (subcutaneous, systemic and intracranial), were established with the Raji B lymphoma cell line expressing either FLuc_green or FLuc_red (as described for *in vitro* experiments). All tumour models were then spectrally imaged with both LH_2 and iLH_2 (**Figure 3, Figure 3 – Figure supplement 1 and Figure 3 – Figure supplement 2**) to obtain the normalised spectra and average radiance of each FLuc mutant with both luciferins in all three *in vivo* models (**Figure 4**). The normalised bioluminescence spectra for every mouse in each model when imaged with LH_2 is shown, with the total radiance for each mouse plotted to the right of the spectral plot (**Figure 4 a-c**). The data shows that when imaged with LH_2 both FLuc_green and FLuc_red had an average peak emission between 610-630nm; meaning the peak emission for FLuc_red is maintained as *in vitro* whereas the peak emission of FLuc_green is red shifted by ~60nm *in vivo*. FLuc_green also exhibited a bimodal spectral distortion, with a minor peak at ~560nm. In contrast to LH_2, FLuc_green and FLuc_red had a ~20nm

separation of average peak emissions in all 3 animal models with iLH_2 (FLuc_green ~700nm and FLuc_red ~720nm) (**Figure 4 d-f**).

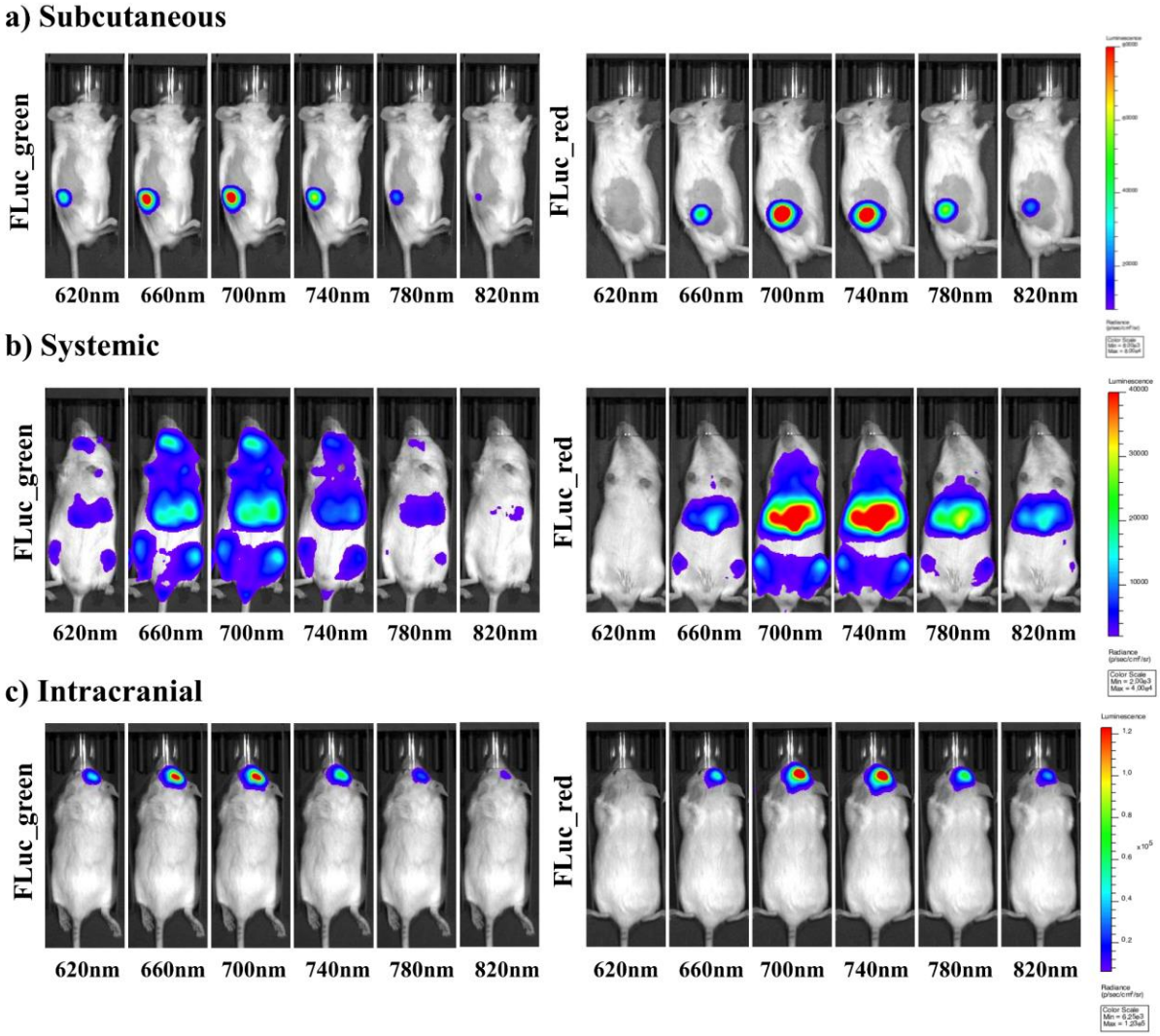

Figure 3: Bioluminescent images of FLuc mutants with iLH$_2$ in vivo

A representative selection of filter images from mice engrafted with the Raji B lymphoma cell line expressing either Fluc_green or Fluc_red for each of the in vivo tumour models when imaged with iLH$_2$ a) subcutaneous b) systemic and c) intracranial (bandpass filters not shown are 600nm, 640nm, 680nm, 720nm, 760nm, 800nm).

Figure 3 – Figure supplement 1 *gives a representative example of all filter images for FLuc_green and FLuc_red acquired in each in vivo model after administration of iLH$_2$.*

Figure 3 – Figure supplement 2 *gives a representative example of all filter images for FLuc_green and FLuc_red acquired in each in vivo model after administration of LH$_2$*

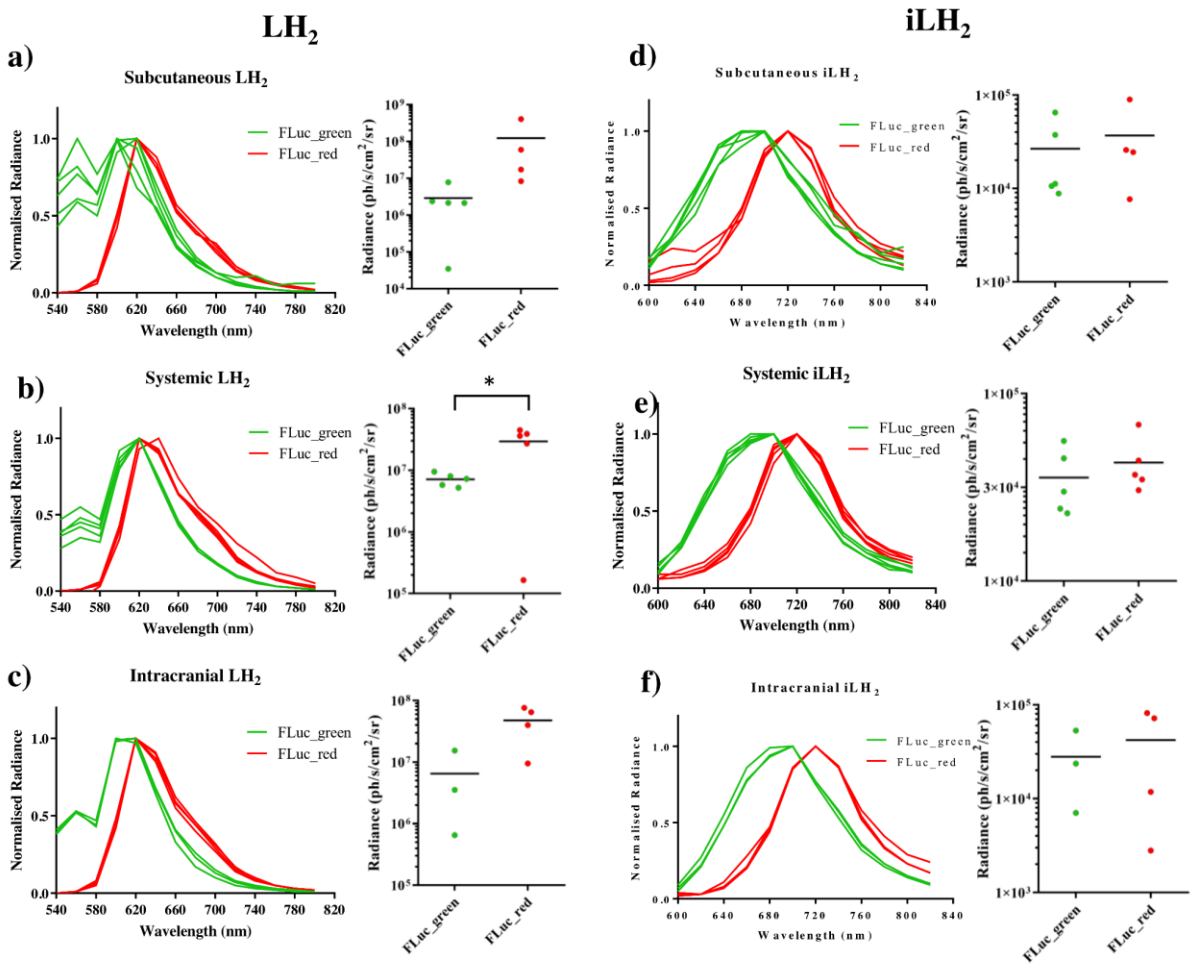

Figure 4: Spectral characterisation of FLuc mutants with LH_2 and iLH_2 in vivo

The normalised spectra, and a plot of average radiance, for each FLuc mutant when expressed in the Raji B lymphoma cell line engrafted in each tumour model when imaged with LH_2 is shown, a) subcutaneous b) systemic and c) intracranial, and when the same animals were imaged with iLH_2 is shown, d) subcutaneous e) systemic and f) intracranial. Subcutaneous (n=9), systemic (n=10), intracranial (n=7). T test used to establish statistical significance comparing average radiance values (systemic model when imaged with LH_2 p = 0.0224).

In addition to the separation of peak emission wavelengths when imaged with iLH_2 *in vivo*, the relative intensities of FLuc_green and FLuc_red were more comparable when imaged with iLH_2 than with LH_2; With LH_2 FLuc_red had an average radiance that was 42 (subcutaneous), 4.12 (systemic) and 7.28 (intracranial) times brighter than FLuc_green (**Figure 4 a-c**). Whereas, when imaged with iLH_2 the average radiance between FLuc_green and FLuc_red was 1.38 (subcutaneous), 1.2 (systemic) and 1.51 (intracranial) times different (**Figure 4 d-f**). No statistically significant difference in relative intensities between FLuc_green and FLuc_red was found in tumour models imaged with iLH_2 ($p = 0.3414$, 0.4594 and 0.6153 for the subcutaneous, systemic and intracranial tumour models respectively, T test). This comparability of relative intensities between FLuc_green and FLuc_red with iLH_2 means that if used as genetic reporters for dual imaging, the dynamic range of radiance values for both enzymes will be more similar, therefore giving a more accurate comparison of the processes being monitored.

Spectral unmixing of firefly luciferase mutants in vivo

To validate the ability to spectrally unmix FLuc_green and FLuc_red *in vivo* with iLH_2 a systemic Raji tumour model was established. Raji cell lines expressing the FLuc mutants were mixed in the following ratios: 90:10, 75:25 and 50:50 for FLuc_green: FLuc_red and vice versa. After spectral BLI with both substrates, animals were sacrificed and the bone marrow was extracted for flow cytometry analysis to confirm the proportions of engrafted Raji FLuc populations (representative examples of flow cytometry plots can be found in **Figure 5 – Figure supplement 1**). Spectral unmixing was performed using Living Image (*Perkin Elmer*) by creating library spectra of FLuc_green and FLuc_red with both LH_2 and iLH_2, established from the pure expressing populations obtained during *in vivo* spectral characterisation (**Figure 4**). Output images with both LH_2 (**Figure 5a**) and iLH_2 (**Figure 5b**)

were generated for FLuc_green and FLuc_red, as well as a composite image for each substrate.

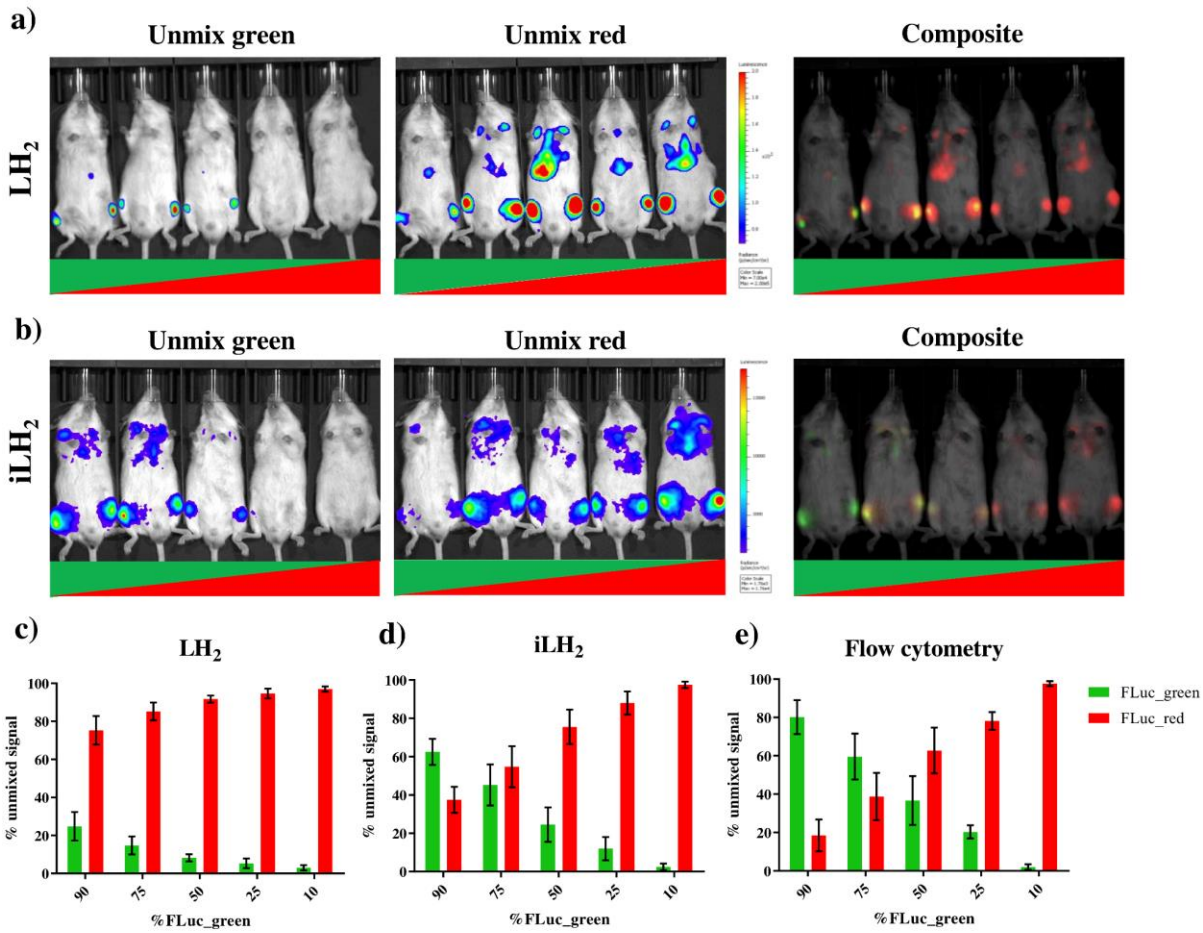

Figure 5: Spectral unmixing of Firefly luciferase mutants in vivo

The Raji B lymphoma cell line expressing either FLuc_green or Fluc_red, were mixed in various proportions and engrafted in a systemic in vivo model. Cell mixtures ranged from 90:10 to 10:90 Fluc_green to Fluc_red, and each imaging session included one mouse engrafted with each mixture. Animals were spectrally imaged with D-Luciferin (LH_2) and infraluciferin (iLH_2) using the IVIS spectrum (Perkin Elmer) in separate imaging sessions.

a) An example of the unmixed Fluc_green, umixed Fluc_red and composite output images when imaged with LH_2 and b) iLH_2. Percentage of unmixed Fluc_green and Fluc_red signal for each cell mixture when imaged with c) LH_2 d) iLH_2, and e) extracted bone marrow samples when analysed by flow cytometry (n = 4 per dilution condition).

***Figure 5 – Figure supplement 1** gives representative flow cytometry plots showing gating of extracted bone marrow sample from a) an FLuc mutant Raji tumour model and from b) a control mouse. c)alsorepresentative flow cytometry plots from a mouse engrafted with each different mixture of mutant FLuc Raji cells (ratio given is Fluc_green: Fluc_red).*

The percentage signal unmixed as FLuc_green and FLuc_red with both LH_2 (**Figure 5c**) and iLH_2 (**Figure 5d**) was determined and correlated to the percentage population of each FLuc_mutant within the Raji cell population taken from extracted bone marrow samples and analysed using flow cytometry (**Figure 5e**). A correlation of 0.99 was found with iLH_2 (R^2 value, SD=0.01). LH_2 had a correlation of 0.89 (R^2 value, SD =0.06), which was significantly different from the R^2 values obtained by flow cytometry ($p < 0.0001$, ONE-Way ANOVA with post hoc Tukey test). No significant difference was found between R^2 values determined by flow cytometry and unmixed bioluminescence signal using iLH_2. Additionally, significant differences were found between the percentage unmixed signal using LH_2 and cellular proportions determined by flow cytometry, with p values of <0.0001, 0.003, 0.0042 and 0.0056 for the 90%, 75%, 50% and 25% FLuc_green conditions respectively. No significant difference was found between percentage unmixed signal using iLH_2 and cellular proportions determined by flow cytometry, except for the 90% FLuc_green condition ($p = 0.0257$). Therefore, iLH_2 is superior to LH_2 for *in vivo* dual reporting applications.

Application of dual bioluminescence imaging using infraluciferin

The characterised and validated *in vivo* dual BLI system using FLuc mutants in combination with iLH_2 was then applied to track tumour burden and CAR T cell therapy within the same animal model. A Raji B lymphoma tumour cell line expressing FLuc_green was used, and healthy human donor T cells were engineered to express CD19 CAR and FLuc_red linked via a 2A peptide. Tumour cells were first systemically engrafted, followed by administration of

CAR T cells 8 days later. A control animal received tumour only. Spectral BLI using iLH_2 was then performed at 3, 4 and 6 days post CAR T cell administration on the IVIS Spectrum.

Output images for the unmixed FLuc_green and FLuc_red signal, as well as the composite of the two unmixed images, for day 6 post CAR T cell administration were generated (**Figure 6a*)***. The radiance values from the unmixed FLuc_green and FLuc_red images for both tumour control and treatment (tumour + CAR T cells) at 3, 4 and 6 days post CAR T cell treatment were determined (**Figure 6b**). As would be expected, the tumour only control showed consistently high levels of FLuc_green signal which increased overtime compared to FLuc_red, which is likely due to the close proximity of Fluc_red photons emitted by the neighbouring treatment mouse. However, the CAR T cell treatment mice initially had a higher proportion of FLuc_green signal, which was then surpassed by FLuc_red by the final imaging. This represents the homing of CAR T cells expressing FLuc_red to the FLuc_green expressing Raji B lymphoma tumour, followed by the expansion of the CAR T cells and the reduction in the tumour growth in the treatment mice.

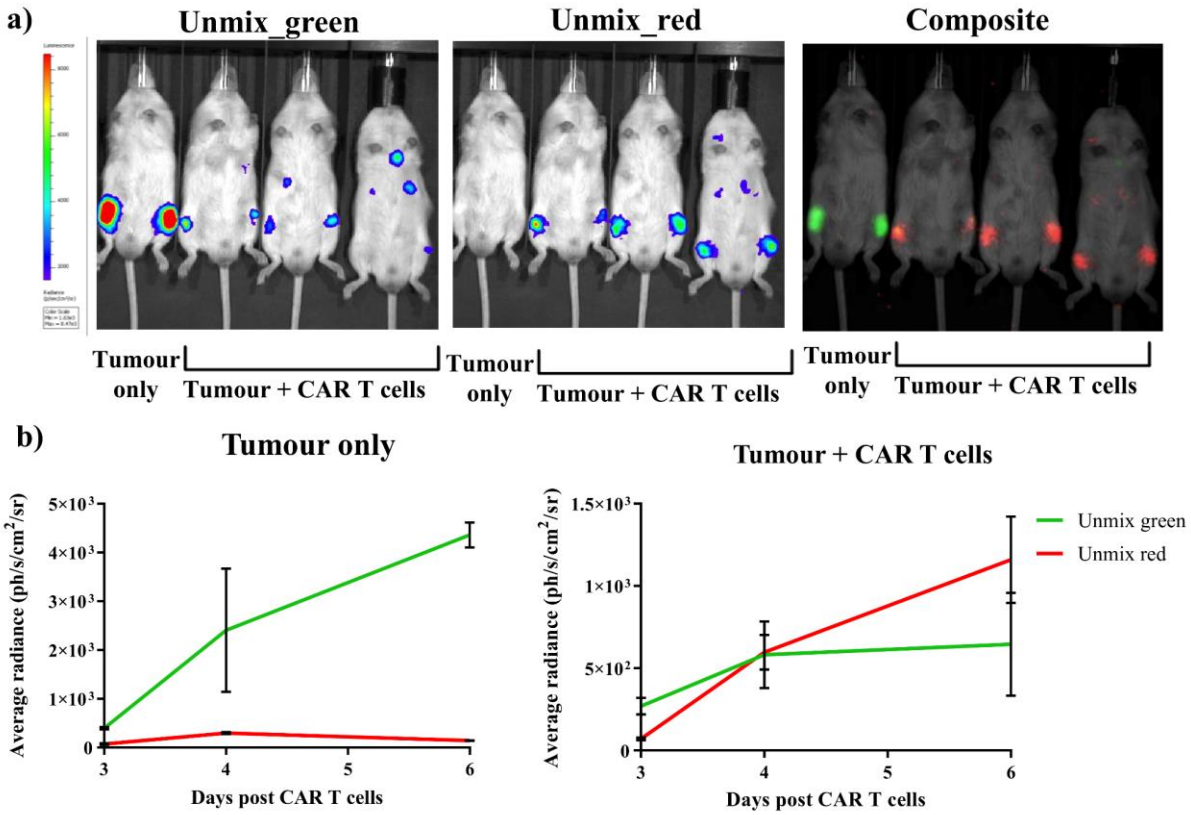

Figure 6: Dual bioluminescence imaging of CAR T cell therapy using infraluciferin

Mice were engrafted with the Raji B lymphoma tumour cell line expressing Fluc_green, and were subsequently treated with healthy human donor T cells engineered to express CD19 CAR and FLuc_red (except the tumour only control). Animals were then spectrally imaged after administration of iLH2 using the IVIS spectrum (Perkin Elmer).

(a) The unmixed Fluc_green images, representing tumour burden, and unmixed Fluc_red images, representing CAR T cell homing, and the composite image are shown for day 6 post CAR T cell treatment.

(b) The average radiance of signal classified as Fluc_green and Fluc_red is plotted for days 3, 4 and 6 post CAR T cell administration for the tumour only control and treatment (tumour + CAR T cells) animals. 3 mice were randomly selected to receive CAR T cell therapy after engraftment was confirmed. Mean and standard deviation plotted. Radiance values from each femur are treated separately (tumour only = 2, treatment =6).

DISCUSSION

Small animal dual (or multi-parameter) bioluminescence is highly desirable. Currently, most dual BLI has been achieved with two luciferases each utilising a different substrate, one of which is normally the auto luminescent coelenterazine [9]. A simpler approach would be to use a single LH_2 substrate and two firefly (or related) luciferases which emit at different wavelengths. This in theory has advantages of higher quantum yield and a more favourable substrate. Such an approach has been attempted: for instance Mezzanotte et al tested dual BLI *in vivo* using LH_2 with the green luciferase (CBG99) with the red luciferase (Ppy RE8) [12]. However, in deeper tissues the shorter wavelength component of green emitting enzyme emission is heavily attenuated by mammalian tissues leaving an "*in vivo* spectrum" which is almost indistinguishable from that of the red luciferase.

To illustrate this, and as a control for subsequent experiments, we attempted dual BLI using a pair of stabilized firefly luciferases, which are green / red shifted to 546nm and 610nm respectively using LH_2 as a substrate [23]. Whilst *in vitro* the spectra could be easily distinguished (**Figure 2)** *in vivo* the spectral separation between the two FLuc enzymes was lost due to the differential attenuation of the green enzyme by biological tissue (**Figure 4**). An obvious solution is to red-shift both enzymes into the optic window while maintaining an adequate separation. However, although bioluminescence emission has been successfully red-shifted through mutagenesis of firefly luciferase the structure of the LH_2 substrate ultimately limits this approach. Dual BLI with a single substrate in the near-infrared should be better; this has been described using BRET based reporters with an coelenterazine derived substrate [24]. To move bioluminescence into the near infrared modification of the LH_2 substrate was required. Indeed, red-shifted luciferin analogues have been reported. These include CycLuc1

and Aka-Lumine, however neither permit variation in emission spectra with different Luciferase mutants [18, 19, 7] (**Figure 2**). More recently, two Naphthyl luciferins, NH_2-$NpLH_2$ and OH-$NpLH_2$, were reported to red shift the *in vitro* bioluminescence emission of CBR to 664nm and 758nm respectively (emission max 614nm with LH_2). Interestingly, NH_2-$NpLH_2$ was shown to have an *in vitro* peak emission of 730nm with an optimised version of CBR (CBR2). The potential application of CBR and CBR2 with NH_2-$NpLH_2$ for dual-BLI *in vivo* was not explored; and the reported broad emission spectrum of optCBR2 in live cells is likely to make any near-infrared dual BLI with NH_2-$NpLH_2$ challenging, however this approach cannot be discounted [20].

We described previously iLH_2, which has a near-infrared emission and in contrast to other LH_2 analogues maintains the 6' hydroxyl benzothiazole group of LH_2 that preserves the colour-shifts of mutant luciferases [14]. Analysis of the x-ray crystal structure of FLuc in complex with the iLH_2 analogue (iDLSA) revealed that the hydrogen-bonding network, thought to be critical in stabilizing the phenolate ion of the emitter, is disrupted in the FLuc-iDLSA due to the accommodation of the larger iLH_2 substrate [25]. This enables full charge delocalization of the phenolate ion, in addition to extended conjugation, resulting in a red-shifted emission as suggested by homology modelling experiments with the recently described near infrared emitting naphthyl analogue [20]. Evidence for the disruption of the network is the absence of a H-bond between Arg337 and Glu311 that is found in the DLSA structures of FLuc and *L. cruciata* Luc. This H-bonding interaction has been proposed to be important for stabilising an active site conformation for green light emission [26]. In addition, the resulting increase in active site polarity due to the rotation of the C-terminal cap could also contribute to the red-shift in light emission [17]. It must be noted that the crystal structure reported here has captured FLuc in the adenylation step of the reaction, therefore further

computational modelling/crystal structure elucidation would be expected to provide further information on the light-emitting step of the reaction with iLH_2 [15, 17] . Finally, the more open adenylation conformation of FLuc -iDLSA may affect the adenylate significantly, altering light production by decreasing the yield of the electronically excited state emitter and/or the efficiency in which the emitter produces a photon. Moreover, small differences in the binding position of the adenylate seen here, caused by positional changes of key active site residues could have a similar effect.

Given that iLH_2 preserves the colour modulation of mutant luciferases (in addition to the 100nm red shift), we set about to explore dual-BLI with iLH_2. We identified two stabilised FLuc enzymes with colour shifting mutations: FLuc_green (V241I/G246A/F250S) and Fluc_red (S284T). Both exhibit a wide separation in peak emission wavelength, and were also balanced in their relative intensities. We next compared *in vitro* spectra with *in vivo* spectra from luciferase expressing cells implanted subcutaneously, systemically and intracranially (to approximate superficial, intermediate and deep light source) with both LH_2 and iLH_2. The near-infrared emission of the FLuc mutants with iLH_2 meant spectral separation was maintained for all animal tumour models. Importantly, the spectra of the two FLuc mutants remained consistent over tissue depth, meaning this dual BLI system could be applied to animal models without prior spectral characterisation. This maintenance of spectral separation, and similarity of relative intensities, between FLuc_green and FLuc_red when imaged with iLH_2 meant this near-infrared bioluminescence system was found to be significantly better at spectral unmixing *in vivo* than using LH_2. This was demonstrated when the unmixed bioluminescent signals were correlated with actual cellular populations, determined by flow cytometry, (R^2 = 0.99 and 0.89 for iLH_2 and LH_2 respectively).

One potential limitation of this system in its current state is the lower quantum yield of the FLuc-iLH$_2$ reaction when compared to the FLuc-LH$_2$ reaction, ~2-3 orders of magnitude dimmer. However, in this study, all mice were successfully spectrally imaged with both LH$_2$ and iLH$_2$, which can be attributed to the sensitivity of the photon counting capabilities of the CCD cameras fitted in optical imagers [27]. The crystal structure reported here will be important for further optimisation of this near-infrared dual BLI system, particularly to increase the brightness of the current enzymes with iLH$_2$, as well as the discovery of novel luciferase colour-mutants which could be used for multi-coloured BLI in the near-infrared. Additionally, the use of this system in combination with luciferases utilising other substrates for multi-coloured BLI could also be explored, as well as its application to monitoring more complex processes in animal models [28]. This work represents an important step forward in increasing the utility of BLI and opens up the window for multi-coloured BLI in the near-infrared.

MATERIALS AND METHODS

Key Resources Table

Reagent type (species) or resource	Designation	Source or reference	Identifiers	Additional information
gene (*Photinus pyralis*)	FLuc	this paper	N/A	Amino acid changes from ref 21 and 23, codon optimised for mammalian expression for use in this paper
strain, strain background (mouse, male)	NSG	Jax™ mouse strain (*Charles River)*	NOD.Cg-*Prkdcscid Il2rgtm1WjI*/SzJ	N/A
cell line (Human, male)	Raji B lymphoma	ATCC® CCL-86™	N/A	Mycoplasma tested by GATC (Eurofins Genomics)
antibody	Anti-human CD34-PE	Biolegend	Clone 581, RRID AB_1731862	(1:20)
antibody	Anti-human CD271-APC	Biolegend	Clone ME20.4, RRID AB_10645515	(1:20)
chemical compound, dye	Viability APC eFluoro780	eBioscience	N/A	(1:1000)
antibody	Anti-mouse/human CD11b PerCP/Cy5.5	Biolegend	Clone M1/70, RRIB AB_893232	(1:20)
antibody	Anti-human CD19 FITC	eBioscience	Clone HIB19, RRID AB_10669461	(1:20)
antibody	Anti-human CD20 eFLuor 450	eBioscience	Clone 2H7, RRID AB_1633384	(1:20)
chemical compound, drug	Luciferin	Regis technologies	N/A	N/A
software, algorithm	Living Image	Perkin Elmer	N/A	N/A

software, algorithm	Prism	Graphpad	N/A	N/A
software, algorithm	Excel	Microsoft	N/A	N/A
software, algorithm	Flow Jo	Tree Star Inc (Oregon, USA)	N/A	N/A
software, algorithm	PyMOL software	Schrodinger	N/A	N/A
software, algorithm	CrysalisPro	Agilent Technologies	N/A	N/A
software, algorithm	BD FACSDIVA	BD biosciences	N/A	N/A
other				
chemical compound, drug	infraluciferin	Anderson, J.C.; Grounds, H.; Jathoul, A.P.; Murray, J.A.H.; Pacman, S.J.; Tisi, L. RSC Advances 2017, 7, 3975-82	N/A	Prepared by JC Anderson laboratory
chemical compound, drug	iDLSA	this paper	N/A	Prepared by JC Anderson laboratory, see supplementary information.
chemical compound, drug	CycLuc1	Merck Millipore	N/A	N/A
chemical compound, drug	Aka-Lumine-HCL	Wako Pure Chemical Industries	N/A	N/A

Preparation of 5'-o-[(n-dehydroinfraluciferyl)-sulfamoyl] adenosine dehydroinfraluciferin

All manipulations were routinely carried out under an inert (Ar or N_2) atmosphere. All reagents were used as received unless stated. For the purposes of thin layer chromatography (tlc), Merck silica-aluminium plates were used, with *uv* light (254 nm) and potassium permanganate or anisaldehyde for visualisation. For column chromatography Merck Geduran® Si 60 silica gel was used. Butyl lithium solutions were standardised with diphenyl acetic acid.

Melting points are uncorrected and were recorded on a Griffin melting point machine. Infrared spectra were recorded using a Bruker Alpha ATR spectrometer. All NMR data was collected using a Bruker AMX 300 MHz or Bruker AVANCE III 600 MHz as specified. Reference values for residual solvents were taken as δ = 7.27 ($CDCl_3$), 2.51 (DMSO –*d*6), 3.30 (MeOD- *d*4) ppm for ^{1}H NMR and δ = 77.2 ($CDCl_3$), 39.5 (DMSO –*d*6), 49.0 (MeOD-*d*4) ppm for ^{13}C NMR. ^{19}F NMR spectra were measured using a Bruker DX300 spectrometer, referenced to trichlorofluoromethane. Coupling constants (*J*) are given in Hz and are uncorrected. Where appropriate COSY and DEPT experiments were carried out to aid assignments. Mass spectroscopy data was collected on a Micromass LCT Premier XE (ESI) instrument. Elemental analysis was performed on an Exeter Analytical Inc. CE-440 CHN analyser.

6-(*β*-Methoxyethoxymethylether)benzothiazole (**1**),[32]

6-(*β*-Methoxyethoxymethyl ether)-2-formylbenzothiazole (**2**),[33]

1-(4-methoxycarbonylthiazole)methyltriphenylphosphonium chloride[34,35]

2',3'-*O*-Isopropylidene-5'-O-sulfamoyladenosine[36] were synthesised using procedures reported in the literature.

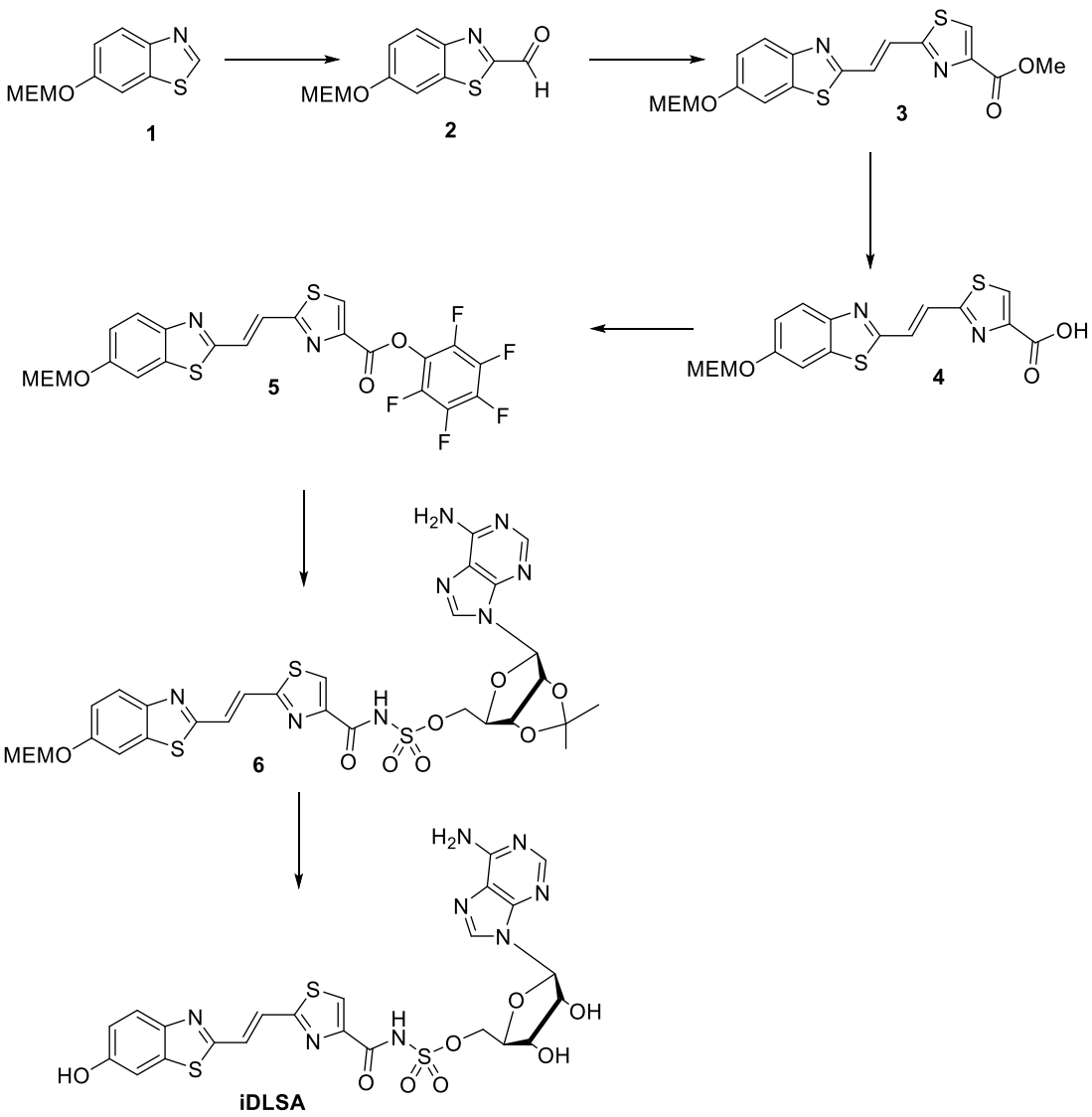

Figure 7: Synthesis of iDLSA

6-(*β*-Methoxyethoxymethoxy)-2-(2-(4-methoxycarbonylthiazol-2-yl)ethenyl) benzothiazole (**3**). A suspension of aldehyde **2** (200 mg, 0.748 mmol) and 1-(4-methoxycarbonylthiazole)methyltriphenylphosphonium chloride (680 mg, 1.50 mmol) in DMF (3.5 mL) was cooled to 0 °C and treated with K_2CO_3 (348 mg, 2.52 mmol). The resultant solution was allowed to warm to rt and stirred for 16 h. After this time H_2O (40 mL) was added and the solution extracted using EtOAc (2 × 40 mL). The organics were combined and washed with H_2O (40 mL), separated, dried ($MgSO_4$), filtered and concentrated *in vacuo*. Purification was achieved using flash column chromatography (60 % Et_2O/Hexane) to give **3** as a mixture of *cis* and *trans* isomers (163 mg, 54 %).

Cis: R_f = 0.52 (60 % EtOAc/Hexane); ^{1}H NMR (600 MHz, $CDCl_3$) δ 3.39 (3H, s, OC*H*$_3$), 3.58-3.59 (2H, m, OC*H*$_2$CH$_2$O), 3.86-3.89 (2H, m, OC*H*$_2$CH$_2$O), 4.00 (3H, s, OC*H*$_3$), 5.36 (2H, s, OC*H*$_2$O), 6.96 (1H, d, *J* = 12.8, C*H*C(N)S), 7.25-7.29 (2H, m, Ar*H*, C*H*C(N)S), 7.62 (1H, d, *J* = 2.3, Ar*H*), 8.06 (1H, d, *J* = 8.9, Ar*H*), 8.28 (1H, s, C*H*S). In $CDCl_3$ solution the *trans* isomer was seen to isomerise to the *cis* isomer.

Trans: A pure sample of *trans* was by separated by column chromatography to give **3** as a yellow solid. m.p. 112-115 °C; R_f = 0.48 (60 % EtOAc/Hexane); IR ν_{max} 3101, 2926 (ν_{CH}), 2889 (ν_{CH}), 2818 (ν_{CH}), 1716 (ν_{CO}), 1629, 1598, 1556, 1495, 1456, 1333, 1318, 1281, 1239, 1222, 1208, 1162, 1089, 1046, 978 cm^{-1}; ^{1}H NMR (600 MHz, $CDCl_3$) δ 3.39 (3H, s, OC*H*$_3$), 3.58-3.59 (2H, m, OC*H*$_2$CH$_2$O), 3.86-3.88 (2H, m, OC*H*$_2$CH$_2$O), 4.00 (3H, s, OC*H*$_3$), 5.35 (2H, s, OC*H*$_2$O), 7.22 (1H, dd, *J* = 8.9, 2.4, Ar*H*), 7.59 (1H, d, *J* = 2.4, Ar*H*), 7.68 (2H, s, C*H*C(N)S), 7.92 (1H, d, *J* = 8.9, Ar*H*), 8.21 (1H, s, C*H*S); ^{13}C NMR (150 MHz, $CDCl_3$) δ 52.8 (CH_3), 59.2 (CH_3), 68.0 (CH_2), 71.7 (CH_2), 94.0 (CH_2), 107.5 (CH), 117.9 (CH), 124.1 (CH), 128.2 (CH), 128.7 (CH), 136.2 (C), 148.1 (C), 148.9 (C), 156.3 (C), 161.7 (C), 162.9 (C), 165.6 (C); m/z (ESI) 407 (100%, M^++H); HRMS $C_{18}H_{19}N_2O_5S_2$ calcd. 407.0735, found 407.0738.

(*E*)-6-(*β*-Methoxyethoxymethoxy)-2-(2-(4-carboxythiazol-2-yl)ethenyl) benzothiazole (**4**). A suspension of **3** (20 mg, 0.049 mmol) in THF (0.75 mL) and H_2O (0.37 mL) was treated with LiOH.H_2O (5.0 mg, 0.12 mmol) and stirred for 15 min. After this time H_2O (10 mL) and EtOAc (10 mL) were added and the layers separated. The aqueous layer was acidified with 2 M HCl and extracted using EtOAc (2 × 10 mL), organics dried over $MgSO_4$, filtered and concentrated *in vacuo* to give **4** (19 mg, quant.) as a yellow solid. m.p. 175-178 °C; R_f = 0.20 (50 % EtOAc/MeOH); IR ν_{max} 3101 (ν_{OH}), 2917 (ν_{CH}), 1680 (ν_{CO}), 1598, 1554, 1455, 1398, 1320, 1241, 1204, 1160, 1101, 1045, 938 cm^{-1}; ^{1}H NMR (600 MHz, MeOD-*d*4) δ 3.33 (3H, s, OC*H*$_3$), 3.57-3.58 (2H, m, OC*H*$_2$CH$_2$O), 3.84-3.85 (2H, m, OC*H*$_2$CH$_2$O), 5.36 (2H, s, OC*H*$_2$O), 7.25 (1H, dd, *J* = 8.9, 2.4, Ar*H*), 7.69 (1H, d, *J* = 2.4, Ar*H*), 7.71 (1H, dd, *J* = 16.1, 0.6, C*H*C(N)S), 7.73 (1H, d, *J* = 16.1, C*H*C(N)S), 7.80 (1H, d, *J* = 8.9, Ar*H*), 8.43 (1H, s, *J* = 7.5, C*H*S); ^{13}C NMR (150 MHz, MeOD-*d*4) δ 59.1 (CH_3), 69.0 (CH_2), 72.8 (CH_2), 95.0 (CH_2), 108.7 (CH), 119.0 (CH), 124.7 (CH), 128.5 (CH), 129.1 (CH), 130.1 (CH), 137.5 (C), 149.8 (C), 150.0 (C), 157.7 (C), 163.8 (C), 164.6 (C), 166.7 (C); m/z (ESI) 393 (100%, M^++H), 300 (9%); HRMS $C_{17}H_{17}N_2O_5S_2$ calcd. 393.0579, found 393.0581; Anal. Calcd. for $C_{17}H_{16}N_2O_5S_2$: C, 52.03; H, 4.11; N, 7.14. Found C, 51.85; H, 4.29; N, 6.71 %.

6-(*β*-Methoxyethoxymethoxy)-2-(2-(4-pentafluorophenoxycarbonylthiazol-2-yl)ethenyl) benzothiazole (**5**). A solution of **4** (30 mg, 0.077 mmol) in pyridine (3.80 mL) was treated with EDC (18 mg, 0.096 mmol) and pentafluorophenol (18 mg, 0.096 mmol) and stirred at rt for 16 h. The reaction mixture was concentrated *in vacuo*. Purification was achieved using flash column chromatography (30 % Et_2O/hexane) to give **5** as a yellow solid (37 mg, 86 %). m.p. 87-91 °C; R_f = 0.25 (30 % EtOAc/Pet. Ether); IR ν_{max} 2922, 2887, 2835, 1764 (ν_{CO}), 1599, 1554, 1486, 1470, 1454, 1321, 1290, 1260, 1242, 1211, 1199, 1180, 1137, 1123, 1100, 1060, 1010, 986 cm^{-1}; ^{1}H NMR (600 MHz, $CDCl_3$) δ 3.40 (3H, s, OC*H*$_3$), 3.59-3.60 (2H, m, OC*H*$_2$CH$_2$O), 3.87-3.88 (2H, m, OC*H*$_2$CH$_2$O), 5.36 (2H, s, OC*H*$_2$O), 7.23 (1H, dd, *J* = 8.9, 2.4, Ar*H*), 7.60 (1H, d, *J* = 2.4, Ar*H*), 7.72 (1H, dd, *J* = 16.2, 0.6, C*H*C(N)S), 7.74 (1H, d, *J* = 16.2, C*H*C(N)S), 7.94 (1H, d, *J* = 9.0, Ar*H*), 8.40 (1H, d, *J* = 0.4, C*H*S); ^{13}C NMR (150 MHz, $CDCl_3$) δ 59.2 (CH_3), 68.0 (CH_2), 71.7 (CH_2), 94.0 (CH_2), 107.5 (CH), 117.9 (CH), 124.3 (CH), 124.9 (C), 127.3 (CH), 129.8 (CH), 131.4 (CH), 136.4 (C), 137.3 (C), 139.0 (C), 140.6 (C), 142.2 (C), 144.7 (C), 149.2 (C), 156.4 (C), 156.8 (C), 162.5 (C), 166.6 (C); ^{19}F NMR ($CDCl_3$, 282) δ -150.0 (d, *J* = 16.9, Ar*F*), -157.14 (app t, *J* = 19.7, Ar*F*), -161.9 (dd, *J* = 19.7, 16.9, Ar*F*); m/z (ESI) 559 (100%, M^++H); HRMS $C_{23}H_{15}F_5N_2O_5S_2$ calcd. 559.0415, found 559.0418.

2',3'-*O*-Isopropylidene-5'-*O*-*[N*-(6-(*β*-methoxyethoxymethoxy)-dehydroinfraluciferyl)-sulfamoyl]adenosine (**6**). A solution of 2',3'-*O*-Isopropylidene-5'-O-sulfamoyladenosine (20 mg, 0.052 mmol) in DMF (1.8 mL) was treated with DBU (11 mg, 0.076 mmol) and stirred at rt for 10 min. A solution of **5** (29 mg, 0.052 mmol) in DMF (0.2 mL) was then added dropwise. The reaction was stirred at rt for 16 h. After this time pyridine (0.15 mL) was added and the solution stirred for 4 h. The resultant solution was concentrated *in vacuo* and purified using flash column chromatography (5 % MeOH/DCM) to give **6** (30 mg, 76 %) as a yellow solid. m.p. 164 °C, dec.; R_f = 0.32 (5 % MeOH/DCM); IR ν_{max} 3290 (ν_{OH}), 2932 (ν_{CH}), 1644 (ν_{CO}), 1598, 1552, 1505, 1457, 1418, 1373, 1291, 1250, 1209, 1150, 1103, 1080, 1048, 985 cm^{-1}; ^{1}H NMR (600 MHz, DMSO-*d*6) δ 1.34 (3H, s, C(C*H*$_3$)$_2$), 1.54 (3H, s, C(C*H*$_3$)$_2$), 3.21 (3H, s, OC*H*$_3$), 3.46-3.49 (2H, m, OC*H*$_2$CH$_2$O), 3.74-3.78 (2H, m, OC*H*$_2$CH$_2$O), 4.09 (1H, dd, *J* = 11.0, 4.9, C*H*$_2$OS(O)$_2$), 4.12 (1H, dd, *J* = 11.0, 4.9,

CH_2OS(O)$_2$), 4.42-4.46 (1H, m, OC*H*CH$_2$), 5.09 (1H, dd, *J* = 6.1, 2.5, C*H*CHO), 5.36 (2H, s, OCH_2O), 5.41 (1H, dd, *J* = 6.1, 2.9, C*H*CHNO), 6.17 (1H, d, *J* = 2.9, CHC*H*NO), 7.22 (1H, dd, *J* = 8.9, 2.5, Ar*H*), 7.35 (2H, br, NH_2), 7.71 (1H, d, *J* = 16.1, C*H*C(N)S), 7.79 (1H, d, *J* = 16.0, C*H*C(N)S), 7.79 (1H, d, *J* = 2.5, Ar*H*), 7.95 (1H, d, *J* = 8.9, Ar*H*), 8.11 (1H, s, C*H*S), 8.12 (1H, s, NC*H*(N)), 8.44 (1H, s, NC*H*(N)); ^{13}C NMR (150 MHz, DMSO-*d*6) δ 25.2 (CH$_3$), 27.1 (CH3), 58.1 (CH$_3$), 67.3 (CH$_2$), 67.6 (CH$_2$), 71.0 (CH$_2$), 81.6 (CH), 83.5 (CH), 83.9 (CH), 89.3 (CH), 93.3 (CH2), 108.0 (CH), 113.2 (C), 117.4 (CH), 118.8 (C), 123.6 (CH), 125.2 (CH), 126.1 (CH), 128.5 (CH), 136.0 (C), 139.6 (CH), 148.6 (C), 149.0 (C), 152.8 (CH), 155.3 (C), 156.1 (C), 156.8 (C), 162.8 (C), 162.9 (C), 165.0 (C); m/z (ES$^+$) 761 (100%, M$^+$+H); HRMS $C_{30}H_{30}N_8O_{10}S_3$ calcd. 761.1482, found 761.1486.

6-Hydroxy-2-(4-1E,3E-(4-ethoxycarbonyl-4,5-dihydrothiazol-2-yl)buta-2,4-dienyl)benzothiazole (iDLSA). A solution of **6** (20 mg, 0.026 mmol) in TFA (0.32 mL) was stirred at rt for 2 h and then H_2O (0.1 mL) added and the solution concentrated *in vacuo*. EtOH (2 mL) added and concentrated *in vacuo* to give the TFA salt of iDLSA (18 mg, 94 %) as an orange solid. m.p. 68-70 °C; IR ν_{max} 3102 (ν_{OH}), 1667 (ν_{CO}), 1426, 1132 cm^{-1}; ^{1}H NMR (600 MHz, DMSO-*d*6) δ 4.20-4.25 (2H, m, C*H*OH, C*H*OH), 4.53-4.59 (3H, m, C*H*OC, CH_2OS(O)$_2$), 5.96 (1H, d, *J* = 5.0, CHC*H*NO), 7.00 (1H, d, *J* = 2.4, Ar*H*), 7.42 (1H, d, *J* = 2.5, Ar*H*), 7.72 (1H, d, *J* = 15.9, C*H*C(N)S), 7.84 (1H, d, *J* = 8.8, Ar*H*), 7.95 (1H, d, *J* = 15.8, C*H*C(N)S), 8.33 (1H, s, C*H*S), 8.53 (1H, s, NC*H*(N)), 8.59 (1H, s, NC*H*(N)). ^{13}C NMR too weak due to poor solubility of compound. MS did not give M+ or meaningful fragment for accurate mass measurement.

Preparation of the P.pyralis luciferase-5'-o-[(n-dehydroinfraluciferyl)-sulfamoyl] adenosine dehydroinfraluciferin (FLuc-iDLSA) complex

Approximately 0.6 mg of iDLSA was suspended in 500 µL of crystallization buffer (25 mM Tris-Cl containing 200 mM AmSO4, 1 mM DTT, 1 mM EDTA) pH 7.85 at 21°C. The solution was vortexed vigorously and sonicated. Most of the solid was dissolved and the concentration was determined to be ~1 mM by UV absorbance (using an extinction

coefficient of 8200 at 372 nm for this buffer and pH). A 20 mg/mL solution of *P. pyralis* luciferase (PpyWT that contains the N-terminal peptide GPLGS-) in the same buffer (500 µL) was mixed gently with the iDLSA at room temperature and then incubated at 15°C for 20 min. The concentration of iDLSA in the protein-inhibitor mixture was determined by UV absorbance to be 620 µM, giving an inhibitor:enzyme ratio of ~3:1, at this point the bioluminescence activity of the mixture was assayed and the enzyme was 85% inhibited. A small amount of a separate iDLSA solution (available from solubility trials) was added to bring the inhibitor:enzyme ratio to ~4:1, and based on activity the enzyme was 91% inhibited. Finally, the protein-inhibitor solution was added to ~0.5 mg of iDLSA and mixed gently and incubated at 15 °C for 15 min. Based on activity, 99% of the enzyme was inhibited and based on UV absorbance the inhibitor:enzyme ratio was 5.6:1 (950 µM:170 µM) The protein-inhibitor solution was centrifuged and a very slight amount of inhibitor was evident. The supernatant was frozen in liquid nitrogen in ~ 18-50µL aliquots and stored at -80°C. A single aliquot was thawed and the solution remained clear. The pH of this solution at 6°C should be 8.3, pH 8.17 at 10°C, and pH 7.9 at 21°C.

Crystallisation and refinement of P. pyralis luciferase/dehydroinfraluciferin DLSA complex

Approximately 0.6 mg of iDLSA was resuspended in 500µL of buffer (25mM Tris-Cl containing 200mM $(NH_4)_2SO_4$, 1mM DTT, 1mM EDTA) pH 7.85 at 21°C to a concentration of 1mM as determined by UV absorbance (extinction coefficient of 8200 at 372 nm). This solution was mixed with a 20 mg/mL solution of *P. pyralis* (inhibitor:enzyme ratio of ~3:1) at room temperature and then incubated at 15 °C for 20 min. The inhibitor:enzyme solution was centrifuged and the supernatant was frozen in liquid nitrogen in ~ 18 - 50 µL aliquots and stored at -80 °C for future crystallisations.

669

670 Crystallizations used the hanging drop vapour diffusion method. Drops containing 1-2 µl of
671 inhibitor:enzyme solution were mixed with the same volume of well solution and equilibrated
672 against 500 µl of well solution, incubated at 4 °C, with crystals typically appearing within 48
673 hours. Glycerol was used as a cryoprotectant, in an optimized well solution of 150 mM
674 $(NH_4)_2SO_4$, 50 mM HEPES pH 7.0, 2% PEG 1000.

675

676 Data were collected at the Diamond Light Source on beam line IO4-1, at wavelength
677 0.91587Å, and 100 K. Processing and data reduction were carried out on site using
678 CrysalisPro (*Agilent Technologies*), and synchrotron data sets were processed and scaled by
679 using XDS, SCALA and XIA2 programs. Molecular replacement methods were used
680 successfully to determine the relative orientation and position of the two monomers in the
681 asymmetric unit using the PHASER program [29]. The starting dehydroinfraluciferin DLSA
682 complex model was derived from the Firefly luciferase apo structure (PDB-ID 3IEP) with all
683 solvent atoms and the luciferin removed. A simple rigid body refinement was sufficient to
684 initiate refinement, with subsequent refinement and model building cycles performed using
685 Refmac5 and Coot [30,31].

686

687 ***Firefly luciferase mutants and cell lines***

688 FLuc mutants contained 11 pH and temperature stabilising mutations
689 (F14R/L35Q/A105V/V182K/T214C/I232K/D234G/E354R/D357Y/S420T/F465R) [21].
690 FLuc_green contained an additional 3 mutations (V241I/G246A/F250S), and FLuc_red has
691 the red-shifting mutation S284T, as well as the mutation R354I which is required to maintain
692 the red-shift in this stabilised FLuc backbone [23]. All FLuc mutants were codon optimised for

mammalian expression and cloned into the MLV-based splicing gamma retroviral vector SFG. The Raji B lymphoma cell line used in all experiments was transduced to express a FLuc mutant, and subsequently flow-sorted for pure FLuc expressing populations using a co-expressed marker gene. For tumour cell lines FLuc.IRES was upstream of the marker gene CD34 or dNGFR as indicated. For T cells FLuc.2A_peptide was upstream of the CAR CD19-4G7_HL-CD8STK-41BBZ.

Production of retroviral supernatant

HEK-293T packaging cells were plated at a density of 200'000 cells/ml in 100mm tissue culture dish ~24 hours prior to transfection. Transfections were performed when cells were 50-70% confluent. A bulk transfection mixture was prepared where 30µl GeneJuice® Transfection Reagent (*Merck millipore*) was added to 470µl of plain RPMI for each supernatant to be produced. Following a 5 minute incubation at room temperature, a total volume of 12.5µg of DNA was added for each plate to be transfected (for retroviral transfection: 3.125µg RDF RD114 env plasmid, 4.6875µg PeqPam-env gagpol plasmid, 4.6875µg SFG retroviral construct). Following addition of plasmid DNA, the mixture was incubated for a further 15 minutes at room temperature prior to dropwise addition to the HEK- 293T cell culture. Plates were gently agitated following transfection. Supernatant harvested at 48 hours was stored at 4°C, and was then combined with the 72 hour harvest prior to aliquoting and storage at -80°C.

Transduction of cell lines

The day prior to transduction Raji B lymphoma cells (atcc® ccl-86™) (>90% viable) were diluted ~1 in 10 to ensure exponential growth for transduction; also a well of non-tissue culture treated 24 well plate was coated with 8µg/ml retronectin (*Lonza*) for every plasmid to

be transduced and left at 4°C overnight. The next day retronectin was aspirated and 250µl of each retroviral supernatant for transduction was added to a well and incubated for 30 minutes at room temperature. Whilst incubating, Raji cells were harvested, counted and resuspended at a concentration of 600,000 cells/ml. supernatants were aspirated from wells of retronectin coated plate and 500µl of cell suspension was added to each well followed by 1.5ml of the same retroviral supernatant that was previously incubated in each well. Cells were spin transduced at 1000 RCF for 40 minutes then returned to incubator for 48 hours before harvest and expression testing.

Flow cytometry and Fluorescence Activated Cell Sorting

Transduction efficiencies were assessed by flow cytometry, based on marker gene expression as indicated by antibody staining using the BD LSR Fortessa™X-20. If necessary Fluorescence Activated Cell Sorting (FACS) was performed to obtain pure expressing populations, also based on marker gene expression as indicated by antibody staining, using the BD FACS Aria™ Fusion. FACS was also use to sort populations of cells expressing differing levels of FLuc_green and FLuc_red within the same cell. Concentration of antibody used was guided by manufacturer's instructions. Anti-human CD34-PE (clone 581), anti-human CD271-APC (clone ME20.4) and anti-mouse/human CD11B-PerCP/Cy5.5 (clone M1/70) (*Biolegend*). Anti-humanCD19-FITC (clone HIB19), anti-human CD20-eFluor450 (clone 2H7) and Viability APC-eFluor780 (*eBioscience*). Data was analysed using Flow Jo software (*Tree Star Inc, Oregon, USA*).

Flow cytometry of extracted bone marrow

When bone marrow cells were required for flow cytometry analysis. Following animal sacrifice by CO_2 narcosis and cervical dislocation, the femurs were removed and transferred

to PBS pending cellular harvest. The ends of the femur were snipped off using scissors and the bone was placed in an extraction tube (microfuge tube with holder made from 200µl pipette tip inserted). Tubes were centrifuged at 1000 RCF for 60 seconds. Bone marrow pellet was resuspended in 50µl Ammonium-Chloride-Potassium (ACK) lysing buffer (*Lonza*) and left for 60 seconds at room temperature before washing with PBS and passing through a 70µm filter before pelleting. Samples were blocked 2.4G2 supernatant (rat anti-mouse CD32) supplemented with mouse Ig FcR blocking reagent (*Miltenyl Biotec*) for 30 minutes at room temperature. Cells were washed with PBS and pelleted, followed by each sample being transferred to a well of a U-bottomed 96 well plate before proceeding with antibody staining. An antibody master mix containing all antibodies to be used for staining was prepared in PBS to a total volume of 100µl per sample. Samples were left to stain at room temperature in the dark for 30 minutes. Samples were washed once with PBS, pelleted and transferred to FACS tubes. Beckman Coulter Flow-Check™fluorospheres were used as a stopping gate for flow cytometry analysis. Beads are supplied at $1x10e^{6}$ beads/ml in an aqueous solution containing preservative surfactant. To prevent toxicity to cellular samples, beads were washed once with PBS prior to addition to samples. Following centrifugation (400 RCF for 5 minutes), beads were resuspended in an equal volume of PBS with 10µl of beads added to each sample.

As 6 fluorophores were used for bone marrow analysis, compensation was performed prior to sample acquisition using OneComp eBeads™ (*eBioscience*). Events were kept between 2,000-5,000 events/second, with 1,000 events being recorded per sample, using flow check beads as a stopping gates (10% each sample). Flow cytometry gating first identified the lymphocyte population (FSC-A vs SSC-A), exclusion of doublet cells (SSC-A vs SSC-W); antibodies detailed in ***Flow cytometry and Fluorescence Activated Cell Sorting*** were then used to gate on viable cells, exclude mouse monocyte cells (mCD11b), identify the Raji

tumour cell population (CD19 and CD20) and finally co-expressed marker gene (dNGFR and dCD34).

Preparation of CAR T cells

On day 1 peripheral blood mononuclear cells were isolated from a healthy donor blood using Ficoll-paque density gradient media (*GE Healthcare*). Cells were resuspended at $2x10^6$ /ml and stimulated with 1mg/ml PHA (*Sigma*). On day 2 cells were fed with IL-2 at a concentration of 100 U/ml (*Genscript*). On day 3 cells were transduced as described in ***transduction of cell lines***, with IL-2 at a final concentration of 100 U/ml. On day 6 cells were harvested and resuspended at $1x10^6$/ml with 100 U/ml IL-2 and left to recover for at least 48 hours before *in vivo* injection. Transduction efficiency was measured using flow cytometry.

In vitro bioluminescence assays

For spectrographic testing of FLuc, mutants were stably transduced in the mammalian Raji B-cell lymphoma cell line. For *in vitro* bioluminescence assays cells were harvested, counted and $1x10^6$ cells/well were resuspended in TEM buffer (1M Tris-acetate, 20mM EDTA and 100mM $MgSO_4$ at pH 7.8) and added in triplicate to wells of a black 96-well plate (100µl/well). If mixtures of cells were used, total cell number remained the same. For spectral testing the stage temperature of the IVIS Spectrum was set to 37°C (automatic acquisition mode, FOV 13.2, f/1). iLH_2 was synthesised by UCL Chemistry. Other substrates tested include D-luciferin (*Regis Technologies*), CycLuc1 (*Merck Millipore*) and Aka-Lumine-HCL (*Wako Pure Chemical Industries*). Substrates were dispensed into the wells using a multi-channel pipette (at a final concentration of 300µM). A 2 minute delay was allowed for stabilisation of light output. Images were acquired through all 18 bandpass filters

on the IVIS Spectrum (20nm bandpass, 490nm to 840nm). Living image software (*Perkin Elmer*) was used for ROI analysis of spectral images and spectral unmixing analysis. Image analysis involved placing a ROI over the signal in each well. If a series of spectral images was acquired, the same ROI was placed over the well in every image for each plate. For spectral unmixing analysis, guided spectral unmixing was first used on pure expressing FLuc_green and FLuc_red populations to create a library spectra for each mutant with each substrate. The relevant library spectra was then used to perform spectral unmixing on mixed FLuc_green and FLuc_red populations (or cellular populations expressing both enzymes). Data exported to Excel (*Microsoft*) and Prism (*Graphpad*) for further analysis. Spectra was normalised to peak emission for each FLuc mutant with each substrate. Due to the characterisation nature of these *in vitro* experiments, and the substantial amounts of precious chemicals needed to synthesise iLH_2, it was decided to repeat each *in vitro* experiment twice with 3 replicates

In vivo models

All animal studies were approved by the University College London Biological Services Ethical Review Committee and licensed under the UK Home Office regulations and the Guidance for the Operation of Animals (Scientific Procedures) Act 1986 (Home Office, London, United Kingdom). All of the *in vivo* models used the severely immunocompromised NSG (NOD.Cg *Prkdc*^{scid}*Il2rg*^{tm1Wji}/SzJ) mouse model (JAX™ mouse strain, *Charles River*). Mice were male and aged between 6-8 weeks old. Due to the characterisation, or proof of concept, nature of these experiments, and the substantial amounts of precious chemicals needed to synthesise iLH_2, it was decided to engraft 4-5 mice for every condition in each model to ensure engraftment and survival in a least 3 animals for each condition. Also, no specific toxicity experiments were performed, but no adverse side effects were observed with

818 iLH_2.

819 For engraftment of subcutaneous tumours, FLuc expressing Raji cell lines were counted and
820 $2x10^6$ cells were pelleted for each animal to be injected. Cells were washed twice in PBS
821 before being resuspended in plain RPMI 1% HEPES (*Sigma-Aldrich*) to a concentration of
822 $2x10^7$ cells/ml and were kept on ice ready for injection. Cells were injected subcutaneously
823 (100µl bolus) into a shaved area of the flank. Mice were left at least 5 days for tumour
824 development before imaging.

825

826 For engraftment of systemic tumours, FLuc expressing Raji cell lines were counted and $5x10^5$
827 cells were pelleted for each animal. If mixtures of two different FLuc expressing cell lines
828 were used, total cell number per mouse remained at $5x10^5$ cells. Cells were washed twice in
829 PBS before being resuspended in plain RPMI 1% HEPES to a concentration of $2.5x10^6$
830 cells/ml and were kept on ice ready for injection. Animals were transferred to a warming
831 chamber set at 39-42°C to facilitate peripheral vasodilation prior to intravenous (IV)
832 injections. Mice were placed in a restraint and cells were injected IV (200µl bolus) into the
833 tail vein. Mice were left at least 7 days for tumour development before imaging. For the CAR
834 T cell model $5x10^6$ CAR positive T cells were injected IV (200µl bolus) 8 days after Raji cell
835 engraftment.

836

837 For engraftment of intracranial tumours, FLuc expressing Raji cell lines were counted and
838 $2x10^4$ cells were pelleted for each animal. Cells were washed twice in PBS before being
839 resuspended in PBS to a concentration of $1x10^4$ cells/µl and were kept on ice ready for
840 injection. Intracranial injections were performed using a stereotaxic frame fitted with a
841 hamilton syringe. Cells were injected (2µl bolus) into the right striatum (from bregma 2 mm
842 right, 1mm anterior, 4mm down). Mice were left at least 7 days for tumour development

before imaging.

In vivo bioluminescence imaging

For imaging of *in vivo* models, LH2 and iLH2 was solubilised in sterile PBS and animals were administered with substrate (2mg (or 100mg/kg) of either LH_2 or iLH_2 in 200µl or 400µl bolus respectively) via intraperitoneal (IP) injection. Animals were anaesthetised using 2% Isofluorine (flow rate 1 L/min O_2). Spectral imaging was commenced 10 minutes post IP injection to allow stabilisation of light output. If the same animal was being imaged with both LH_2 and iLH_2, at least 24 hours was left between imaging to allow for full clearance of substrate. *In vivo* bioluminescent images were acquired using IVIS Spectrum (FOV 24, f/1, Medium (8)bin, automatic acquisition mode for imaging with LH_2, FOV 24, f/1, Medium (8)bin, 120 s acquisition, total imaging time 24 mins for imaging with iLH_2). These parameters are calculated to keep the binning, exposure time and f/stop within an optimal range for quantification. Up to 5 animals could be imaged at once and the stage was heated to 37°C. Open filter images were acquired prior to and post spectral imaging to confirm the stability of photon emission during spectral acquisition. Spectral imaging acquired images through 14 and 12 of the 20nm bandpass filters on the IVIS Spectrum depending on substrate used (530-830nm for LH_2 and 590-830nm for iLH_2), starting from the lowest to the highest filter. It was not necessary to acquire images through all filters as the bioluminescent emissions of FLuc mutants did not cover the full spectral range from 490- 850nm. Living image software was used for ROI analysis of spectral images and spectral unmixing analysis. Radiance values for bioluminescence are shown using pseudo-colour scales detailed in each image. Image analysis involved placing an ROI over the tumour signal for every animal in each model. If a series if spectral images were acquired, the same ROI was placed over tumour signal in every image for each mouse. For spectral unmixing analysis, guided spectral

unmixing was first used on pure expressing FLuc_green and FLuc_red populations from spectral characterisation experiments to create a library spectra for each mutant with each substrate. The relevant library spectra was then used to perform spectral unmixing on mixed FLuc_green and FLuc_red populations. Data exported to Excel (*Microsoft*) and Prism (*Graphpad*) for further analysis

Statistical analysis

Where relevant means ± standard deviation of data given. Statistical tests used include T test and ONE-way ANOVA with post hoc Tukey's test for multiple column comparison (*Prism, Graphpad*). Correlation analysis perform using *Microsoft excel*.

ACKNOWLEDGMENTS

We would like to thank Steven Pacman for the synthesis of infraluciferin, and the following masters students for their contributions to the synthesis of iDLSA, Laszlo Berencei (EPSRC vacation bursary) Boyuan Deng and Julia Holm (Erasmus), the MRC based at Imperial College London for the use of their IVIS Spectrum, especially to Dr Alex Sardini, and the core flow cytometry facility at UCL Cancer Institute for the sorting of cell lines. This work was partly funded by the National Science Foundation grant MCB-1410390, Force Office of Scientific Research grant FA9550-18-1-0017, Erba Diagnostics Mannheim and the EPSRC for an industrial CASE award EP/L504889/1 (SJP) and UCL.

COMPETING INTERESTS

The authors declare no competing interests.

FIGURE SUPPLEMENTS

Figure 1 – figure supplement 1 *data collection, phasing and refinement statistics for P. pyralis luciferase/dehydroinfraluciferin DLSA complex*

Figure 1 – figure supplement 2 *^{1}H and ^{13}C spectra for synthetic chemical compounds comparison of FLuc spectra with LH_2 analogues in vitro*

Figure 2 – figure supplement 2 *in vitro* dual bioluminescence imaging within a single cell

Figure 3 – figure supplement 1 *bioluminescent images of FLuc mutants with infraluciferin in vivo*

Figure 3 – figure supplement 2 *bioluminescent images of FLuc mutants with iluciferin in vivo*

Figure 5 – figure supplement 1 *flow cytometry of extracted bone marrow samples*

REFERENCES

1. Xu, T. *et al.* The Expanding Toolbox of In Vivo Bioluminescent Imaging. *Cancer Imaging Diagn.* 150 (2016). doi:10.3389/fonc.2016.00150
2. Paley, M. A. & Prescher, J. A. Bioluminescence: a versatile technique for imaging cellular and molecular features. *MedChemComm* **5**, 255–267 (2014).
3. Mezzanotte, L., van 't Root, M., Karatas, H., Goun, E. A. & Lowik, C. W. G. M. In Vivo Molecular Bioluminescence Imaging: New Tools and Applications. *Trends Biotechnol.* **35**, 640–652 (2017).
4. Yao, Z., Zhang, B. S. & Prescher, J. A. Advances in bioluminescence imaging: new probes from old recipes. *Curr. Opin. Chem. Biol.* **45**, 148–156 (2018).

5. Yeh, H.-W. & Ai, H.-W. Development and Applications of Bioluminescent and Chemiluminescent Reporters and Biosensors. *Annu. Rev. Anal. Chem.* **12**, null (2019).
6. Branchini, B. R. *et al.* Red-emitting luciferases for bioluminescence reporter and imaging applications. *Anal. Biochem.* **396**, 290–297 (2010).
7. Iwano, S. *et al.* Single-cell bioluminescence imaging of deep tissue in freely moving animals. *Science* **359**, 935–939 (2018).
8. Prescher, J. A. & Contag, C. H. Guided by the light: visualizing biomolecular processes in living animals with bioluminescence. *Curr. Opin. Chem. Biol.* **14**, 80–89 (2010).
9. Maguire, C. A. *et al.* Triple Bioluminescence Imaging for In Vivo Monitoring of Cellular Processes. *Mol. Ther. — Nucleic Acids* **2**, e99 (2013).
10. Stacer, A. C. *et al.* NanoLuc reporter for dual luciferase imaging in living animals. *Mol. Imaging* **12**, 1–13 (2013).
11. Rathbun, C. M. *et al.* Parallel Screening for Rapid Identification of Orthogonal Bioluminescent Tools. *ACS Cent. Sci.* **3**, 1254–1261 (2017).
12. Mezzanotte, L. *et al.* Sensitive Dual Color In Vivo Bioluminescence Imaging Using a New Red Codon Optimized Firefly Luciferase and a Green Click Beetle Luciferase. *Plos One* **6**, e19277 (2011).
13. Adams, S. T. & Miller, S. C. Beyond D-luciferin: expanding the scope of bioluminescence imaging in vivo. *Curr. Opin. Chem. Biol.* **21**, 112–120 (2014).
14. Jathoul, A. P., Grounds, H., Anderson, J. C. & Pule, M. A. A Dual-Color Far-Red to Near-Infrared Firefly Luciferin Analogue Designed for Multiparametric Bioluminescence Imaging. *Angew. Chem.-Int. Ed.* **53**, 13059–13063 (2014).
15. Berraud-Pache, R. & Navizet, I. QM/MM calculations on a newly synthesised oxyluciferin substrate: new insights into the conformational effect. *Phys. Chem. Chem. Phys. PCCP* **18**, 27460–27467 (2016).

16. Sundlov, J. A., Fontaine, D. M., Southworth, T. L., Branchini, B. R. & Gulick, A. M. Crystal structure of firefly luciferase in a second catalytic conformation supports a domain alternation mechanism. *Biochemistry* **51**, 6493–6495 (2012).
17. Nakatsu, T. *et al.* Structural basis for the spectral difference in luciferase bioluminescence. *Nature* **440**, 372–376 (2006).
18. Evans, M. S. *et al.* A synthetic luciferin improves bioluminescence imaging in live mice. *Nat. Methods* **11**, 393-+ (2014).
19. Kuchimaru, T. *et al.* A luciferin analogue generating near-infrared bioluminescence achieves highly sensitive deep-tissue imaging. *Nat. Commun.* **7**, 11856 (2016).
20. Hall, M. P. *et al.* Click beetle luciferase mutant and near infrared naphthyl-luciferins for improved bioluminescence imaging. *Nat. Commun.* **9**, 132 (2018).
21. Jathoul, A. *et al.* Development of a pH-Tolerant Thermostable Photinus pyralis Luciferase for Brighter In Vivo Imaging. in *Bioluminescence - Recent Advances in Oceanic Measurements and Laboratory Applications* (ed. Lapota, D.) (InTech, 2012).
22. Branchini, B. R., Southworth, T. L., Khattak, N. F., Michelini, E. & Roda, A. Red- and green-emitting firefly luciferase mutants for bioluminescent reporter applications. *Anal. Biochem.* **345**, 140–148 (2005).
23. Branchini, B. R. *et al.* Thermostable red and green light-producing firefly luciferase mutants for bioluminescent reporter applications. *Anal. Biochem.* **361**, 253–262 (2007).
24. Rumyantsev, K. A., Turoverov, K. K. & Verkhusha, V. V. Near-infrared bioluminescent proteins for two-color multimodal imaging. *Sci. Rep.* **6**, 36588 (2016).
25. Branchini, B. R. *et al.* Cloning of the Orange Light-Producing Luciferase from Photinus scintillansA New Proposal on how Bioluminescence Color is Determined. *Photochem. Photobiol.* **93**, 479–485 (2017).

965 26. Viviani, V. R., Oehlmeyer, T. L., Arnoldi, F. G. C. & Brochetto-Braga, M. R. A new
966 firefly luciferase with bimodal spectrum: identification of structural determinants of
967 spectral pH-sensitivity in firefly luciferases. *Photochem. Photobiol.* **81**, 843–848 (2005).
968 27. Cool, S. K., Breyne, K., Meyer, E., Smedt, S. C. D. & Sanders, N. N. Comparison of In
969 Vivo Optical Systems for Bioluminescence and Fluorescence Imaging. *J. Fluoresc.* **23**,
970 909–920 (2013).
971 28. Kleinovink, J. W. *et al.* A Dual-Color Bioluminescence Reporter Mouse for
972 Simultaneous in vivo Imaging of T Cell Localization and Function. *Front. Immunol.* **9**,
973 3097 (2018).
974 29. McCoy, A. J. *et al.* Phaser crystallographic software. *J. Appl. Crystallogr.* **40**, 658–674
975 (2007).
976 30. Murshudov, G. N. *et al.* REFMAC5 for the refinement of macromolecular crystal
977 structures. *Acta Crystallogr. D Biol. Crystallogr.* **67**, 355–367 (2011).
978 31. Emsley, P., Lohkamp, B., Scott, W. G. & Cowtan, K. Features and development of Coot.
979 *Acta Crystallogr. D Biol. Crystallogr.* **66**, 486–501 (2010).
980 32. Muramoto, H.; Fukuda, K.; Hasegawa, T.; Okamoto, K.; Kotani, T. Benzothiazole
981 Derivatives. US patent 5900426 A1 (1999).
982 33. Anderson, J. C.; Grounds, H.; Jathoul, A. P.; Murray, J. A. H.; Pacman, S. J.; Tisi, L. A
983 Convergent Synthesis and Optical Properties of Near-infrared Emitting Bioluminescent Infra-
984 luciferins. *RSC Adv.* **7,** 3975-3982 (2017).
985 34. Hermitage, S. A.; Cardwell, K. S.; Chapman, T.; Cooke, J. W. B.; Newton, R. An
986 Efficient, Practical Approach to the Synthesis of 2,4-Disubstituted Thiazoles and Oxazoles:
987 Application to the Synthesis of GW475151. *OPRD* **5**, 37-44 (2001).
988 35. Old, D.W. Therapeutic Substituted Lactams. US patent 0269498 (2008)

36. Heathcock, D.; Forsyth, C. J.; Shiba, K.; Musier-Forsyth, K. Synthesis and Aminoacyl-tRNA Synthetase Inhibitory Activity of Prolyl Adenylate Analogs. *Bioorg. Chem.* **24**, 273-289 (1996).

FIGURE 1 -FIGURE SUPPLEMENT 1

Data collection and refinement statistics (molecular replacement)

	Luciferase/iLH2
Data collection	
Space group	P 2_1
Cell dimensions	
a, *b*, *c* (Å)	47.509, 114.016, 101.557
α, β, γ (°)	90.00, 98.18, 90.00
Resolution (Å)	22.5- 3.1 (3.21)
R_{sym} or R_{merge}	22.7 (46.0)
$I / \sigma I$	2.15 (1.1)
Completeness (%)	94.2 (97.2)
Redundancy	2.7 (2.6)
Refinement	
Resolution (Å)	17.85 - 3.1
No. reflections	17435(1328)
R_{work} / R_{free}	27.4/32.0 (0.39/0.42)
No. atoms	
Protein	8428
Ligand/ion	84
Water	0
B-factors	-
Protein	43
Ligand/ion	24
R.m.s. deviations	-
Bond lengths (Å)	0.01
Bond angles (°)	1.417

*Values in parentheses are for highest-resolution shell.

	HJ_2	HJ_3
Data collection		
Space group	P 1 2_1 1	P 1 2_1 1
Cell dimensions		
a, *b*, *c* (Å)	48.3013, 45.9128, 62.4669	49.937, 45.374, 63.828
α, β, γ (°)	90.00, 99.2863, 90.00	90.00, 101.01, 90.00
Resolution (Å)	24-3.5 () *	49-2.69 (2.74-2.69)
R_{sym} or R_{merge}	10.5 ()	5.4% (64%)
I / σI	17.4 ()	10.9 (1.6)
Completeness (%)	99.7 ()	99.9 (97.6)
Redundancy	6.1 ()	3.6 (3.7)
Refinement		
Resolution (Å)	30-3.05	49-3.0
No. reflections	5038	5446
R_{work} / R_{free}	23.0/32.3	24.6/28.5
No. atoms		
DNA	1684	1712
Ligand/ion	2	2
B-factors		
Protein	77	50
Ligand/ion		49
R.m.s deviations		
Bond lengths (Å)	0.008	0.008
Bond angles (°)	1.47	1.56

*Values in parentheses are for highest-resolution shell.

Data collection, phasing and refinement statistics for mad (semet) structures

	Native	Crystal 1 name			Crystal 2 name	
Data collection						
Space group		common #			common #	
Cell dimensions						
a, *b*, *c* (Å)		common #			common #	
α, β, γ (°)		common #			common #	
	Peak	*Inflection*	*Remote*	*Peak*	*Inflection*	*Remote*
Wavelength	#	#	#	#	#	#
Resolution (Å)	#	#	#	#	#	#
R_{sym} or R_{merge}	#	#	#	#	#	#
I / σI	#	#	#	#	#	#
Completeness (%)	#	#	#	#	#	#
Redundancy	#	#	#	#	#	#
Refinement						
Resolution (Å)		common #			common #	
No. reflections						
R_{work} / R_{free}						
No. atoms						
Protein						
Ligand/ion						
Water						
B-factors						
Protein						
Ligand/ion						
Water						
R.m.s deviations						
Bond lengths (Å)						
Bond angles (°)						

*Number of xtals for each structure should be noted in footnote. *Values in parentheses are for highest-resolution shell.

FIGURE 1 - FIGURE SUPPLEMENT 2

COPIES OF 1H AND 13C NMR SPECTRA FOR SYNTHETIC CHEMICAL COMPOUNDS

^{1}H NMR compound **3** Isomeric mixture

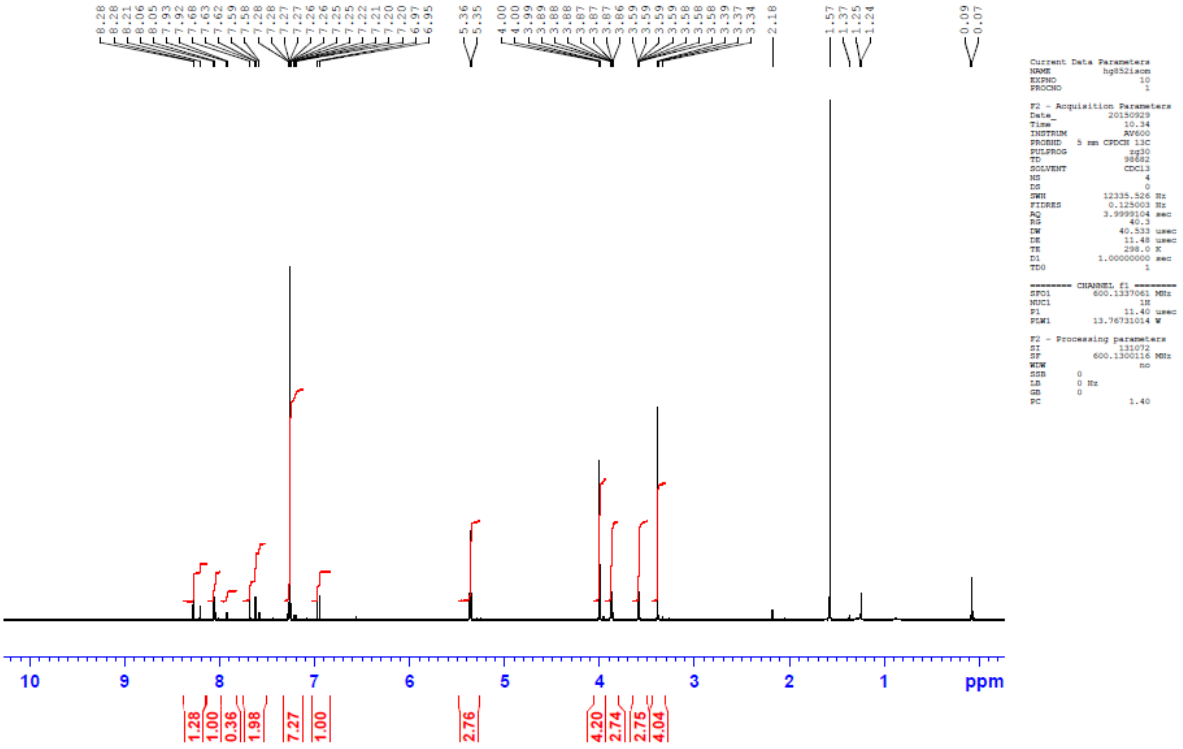

^{1}H NMR compound **3**

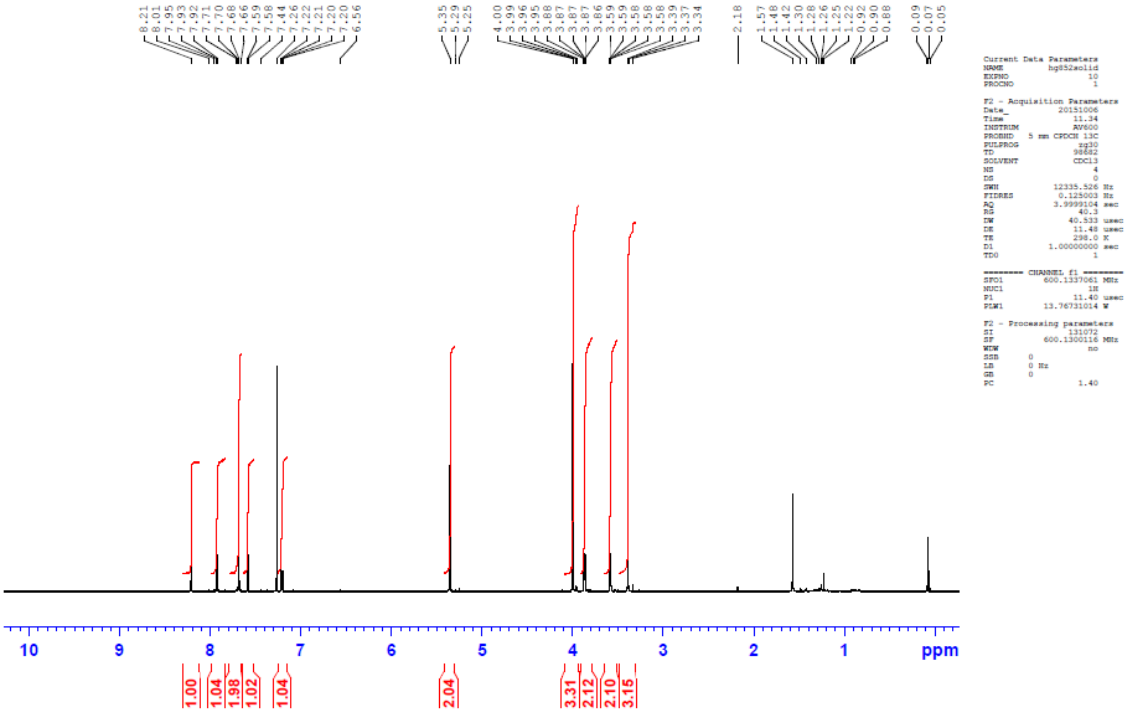

^{13}C NMR compound **3**

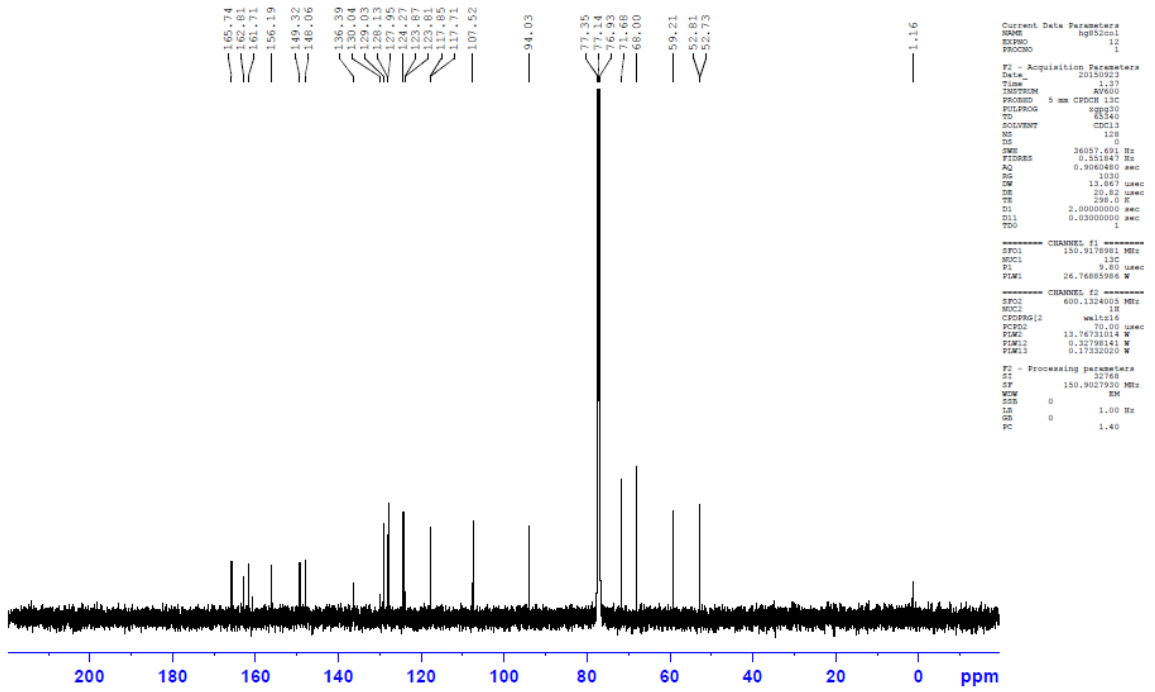

^{1}H NMR compound **4**

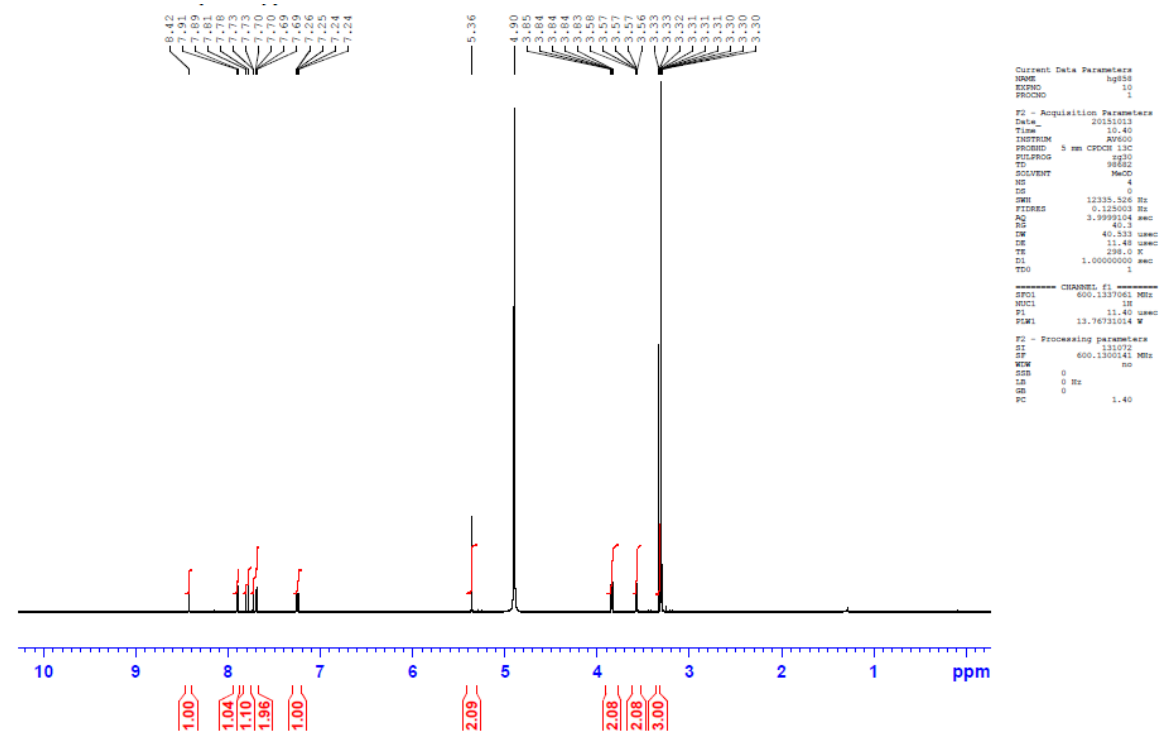

^{13}C NMR compound **4**

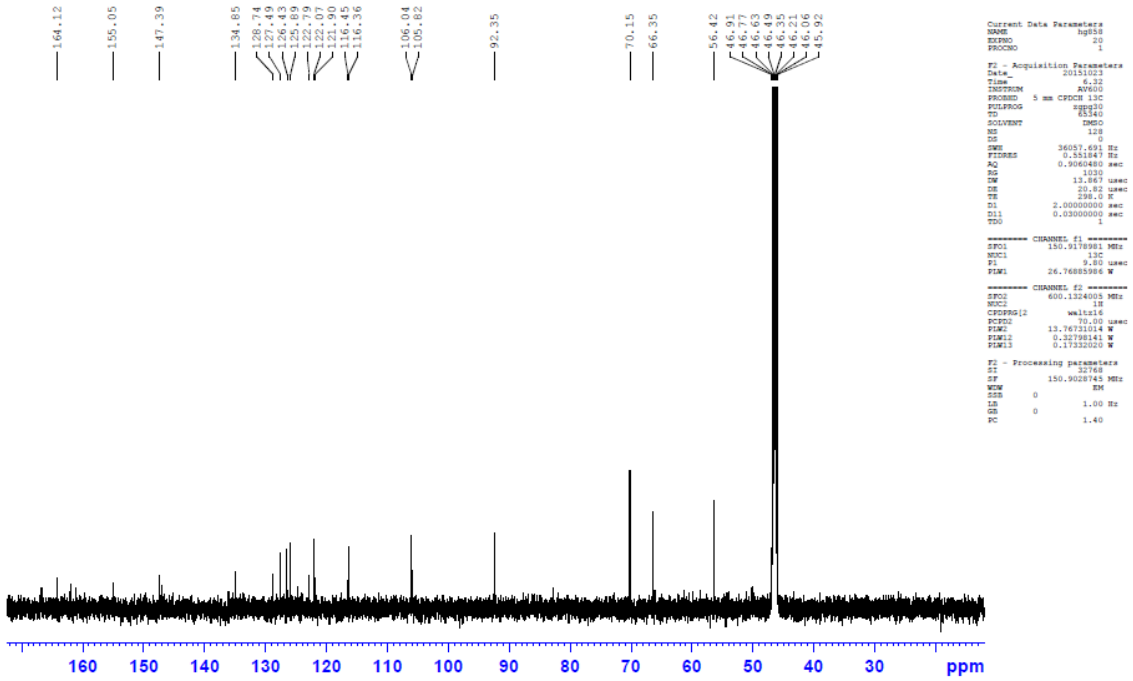

^{1}H NMR compound **5**

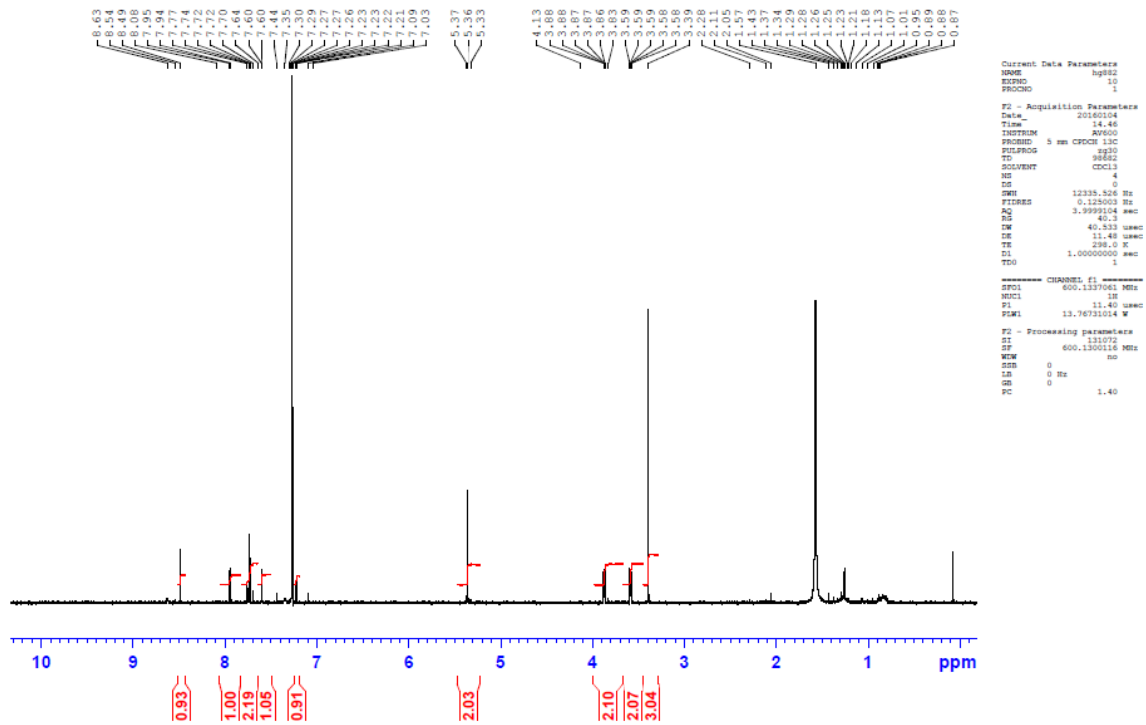

^{13}C NMR compound **5**

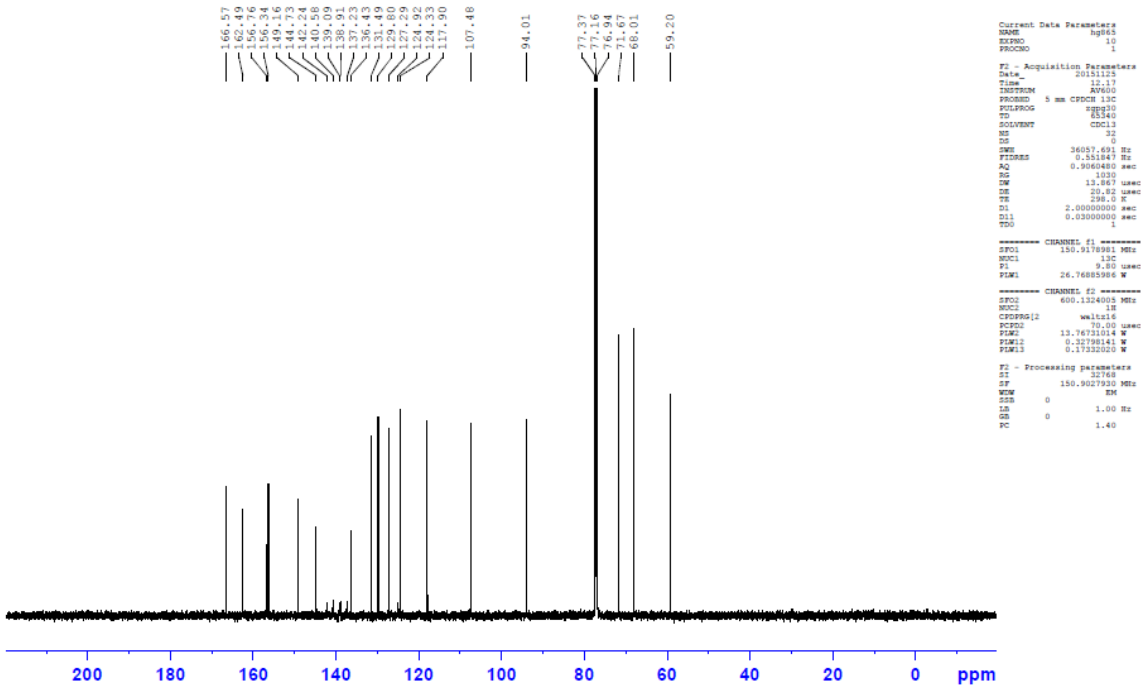

^{1}H NMR compound **6**

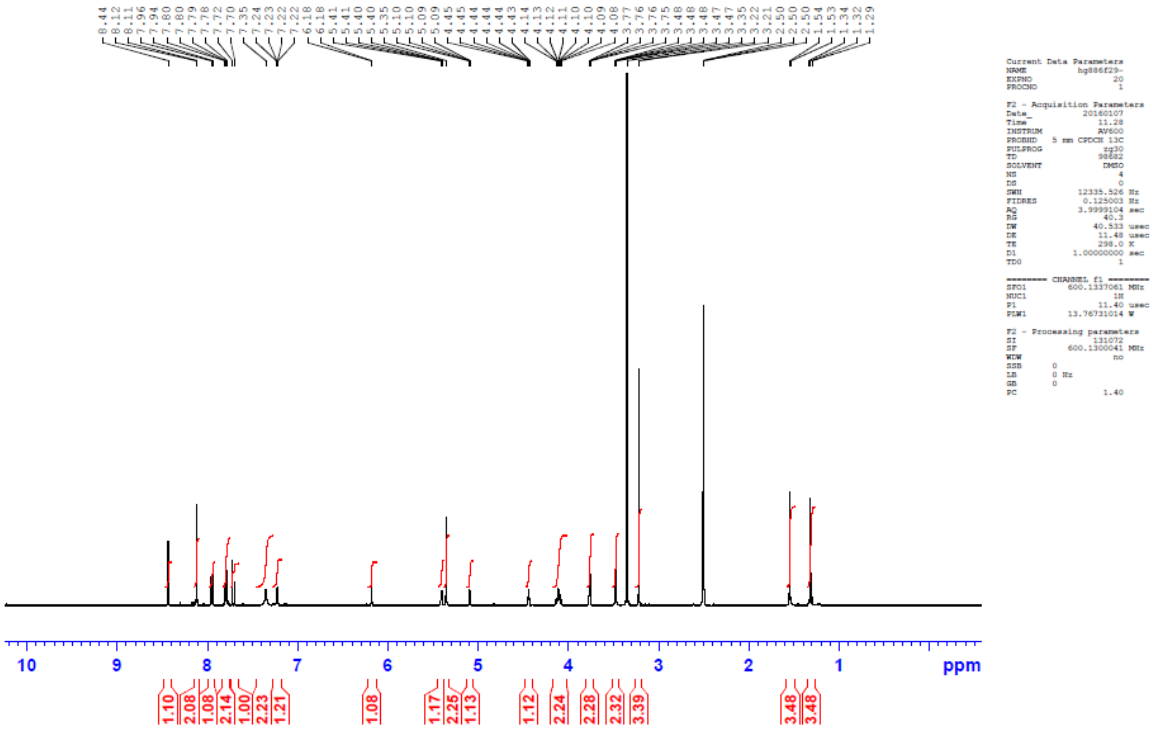

^{13}C NMR compound **6**

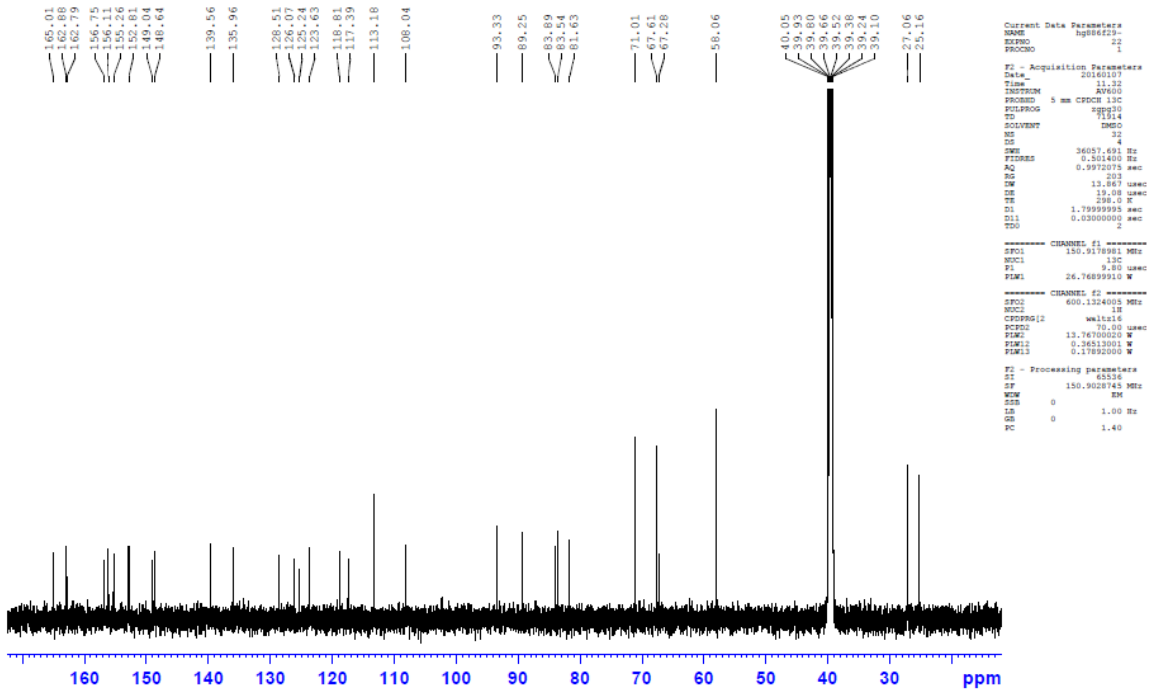

^{1}H NMR compound ***i*DLSA**

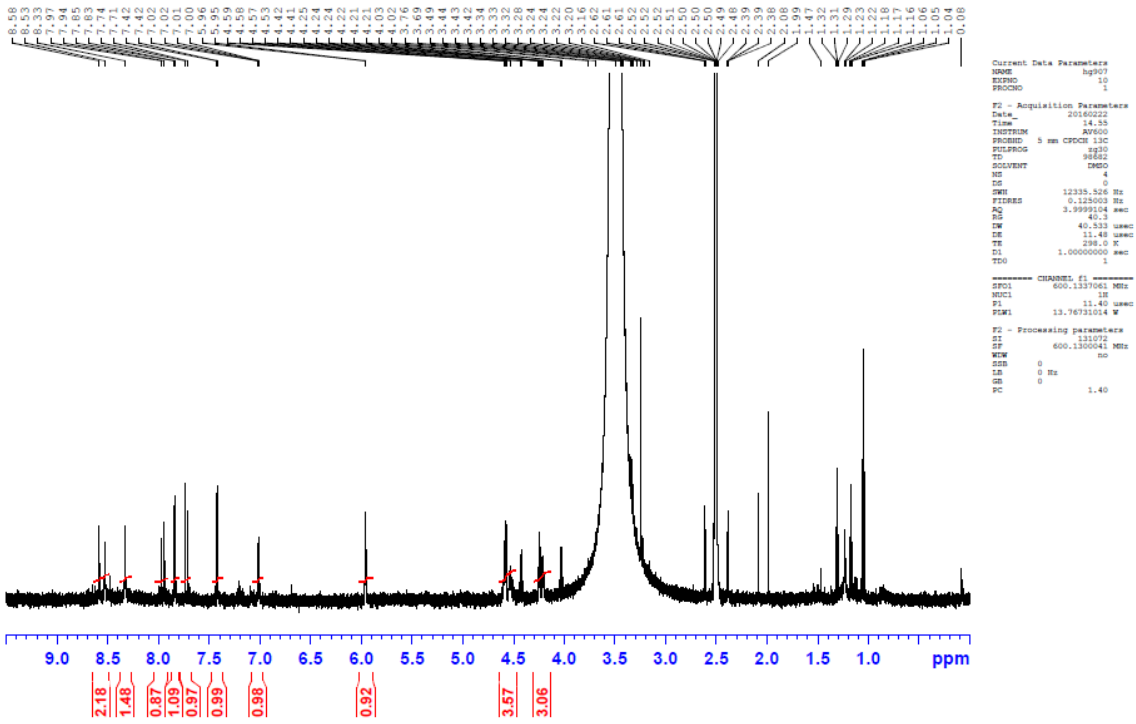

^{1}H NMR compound ***i*DLSA** expansion

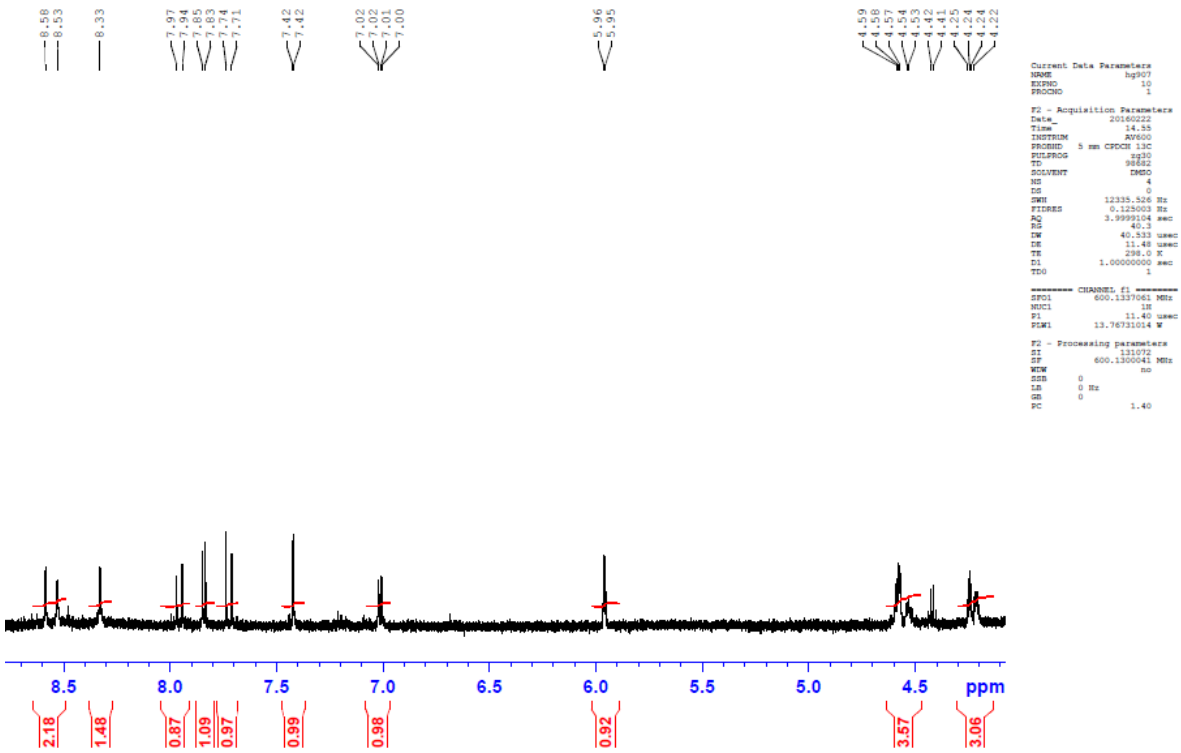

^{13}C NMR compound ***i*DLSA**

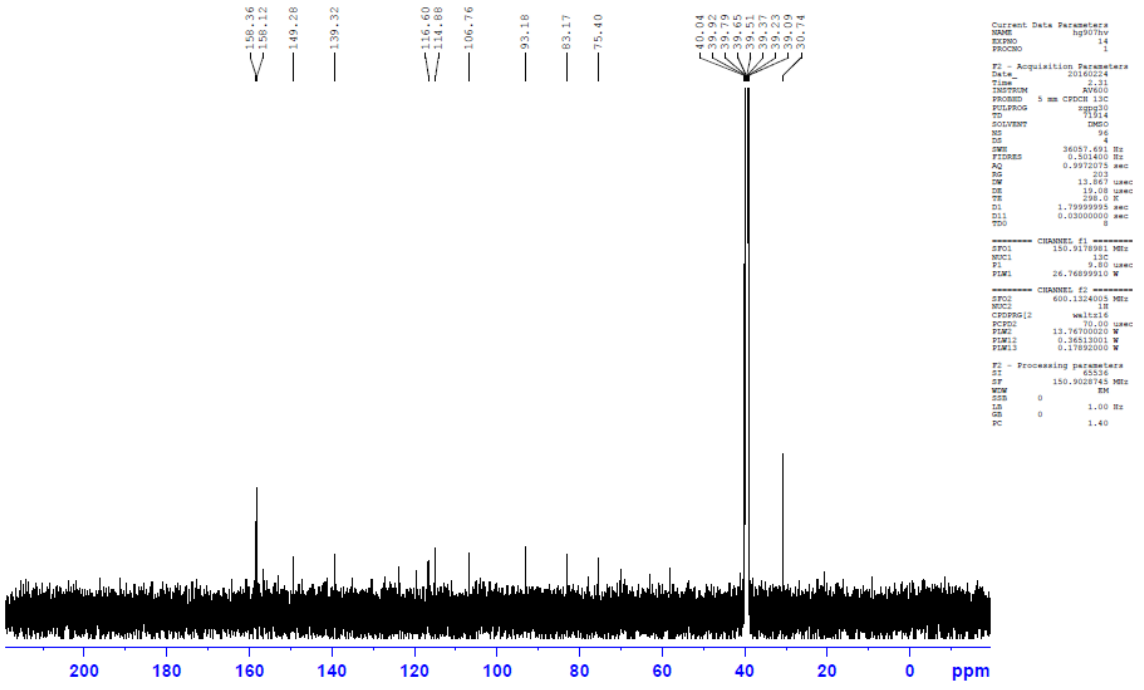

FIGURE 2 – FIGURE SUPPLEMENT 1

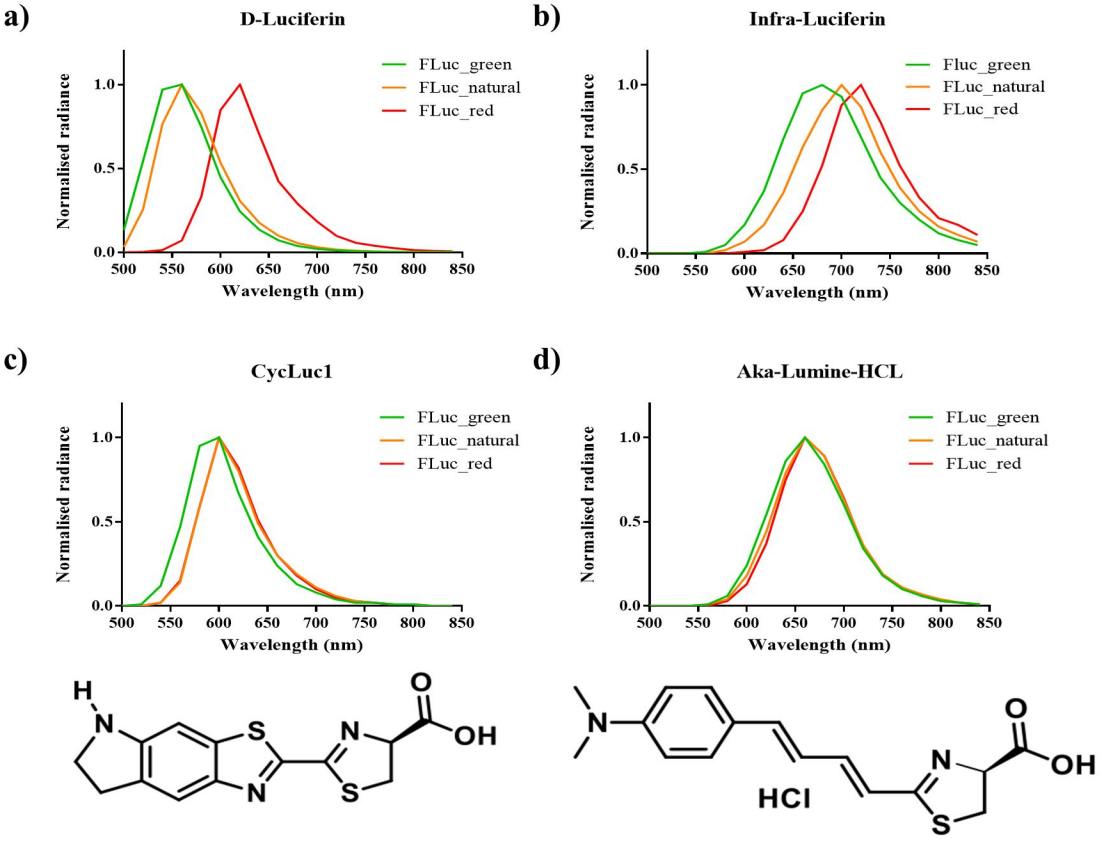

FIGURE 2 – FIGURE SUPPLEMENT 2

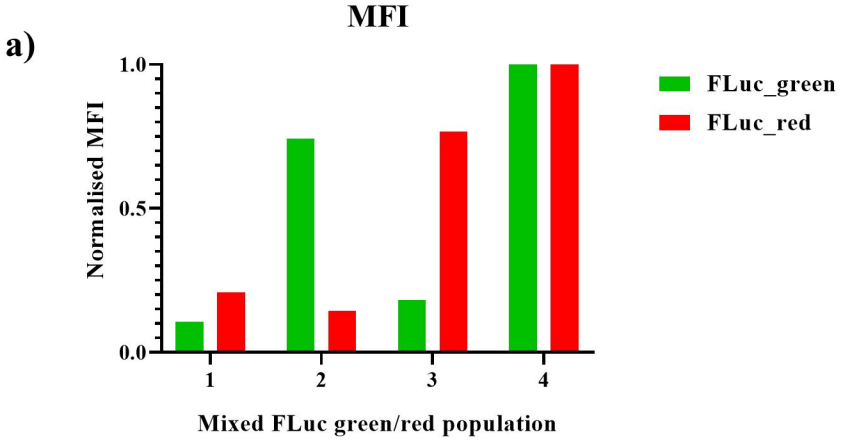

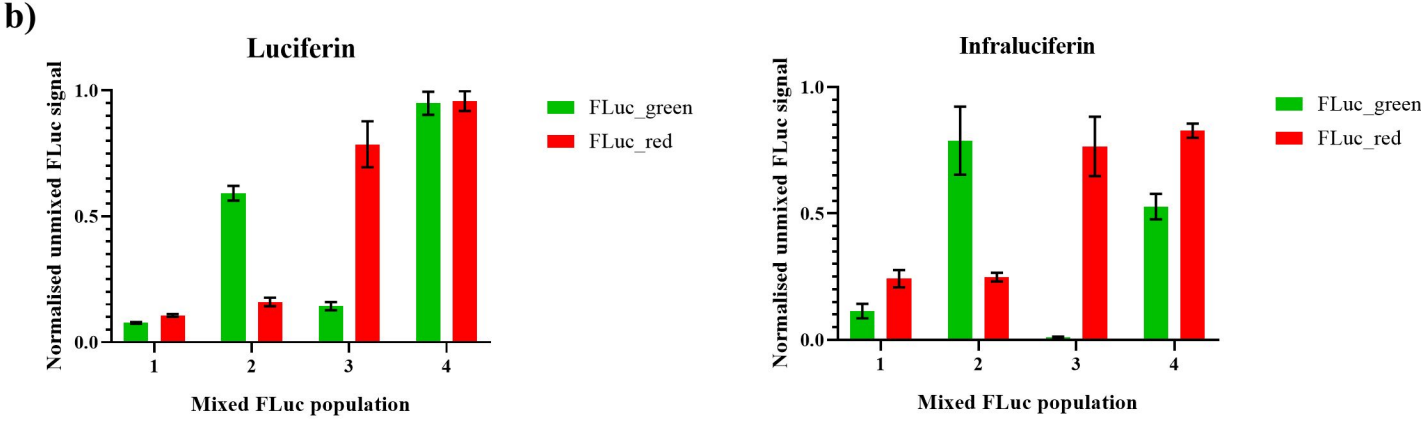

FIGURE 3 – FIGURE SUPPLEMENT 1

iLH$_2$ FILTER IMAGES

Subcutaneous

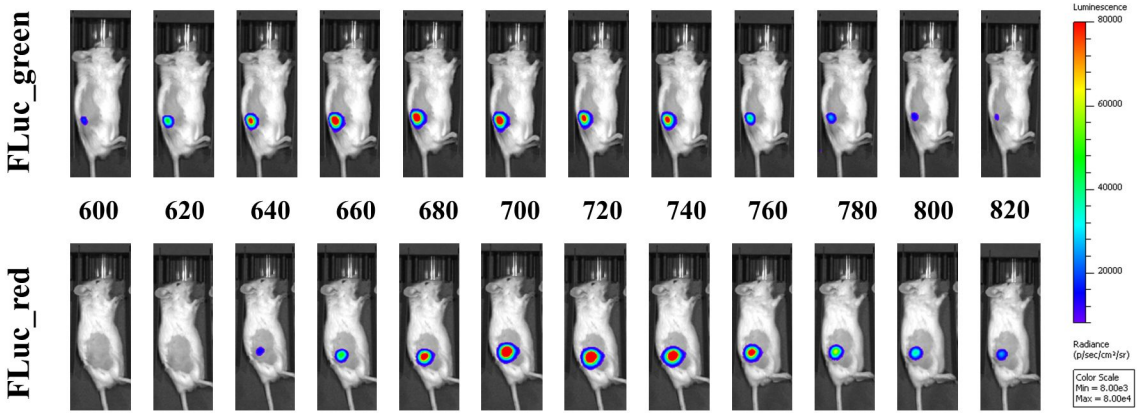

Systemic

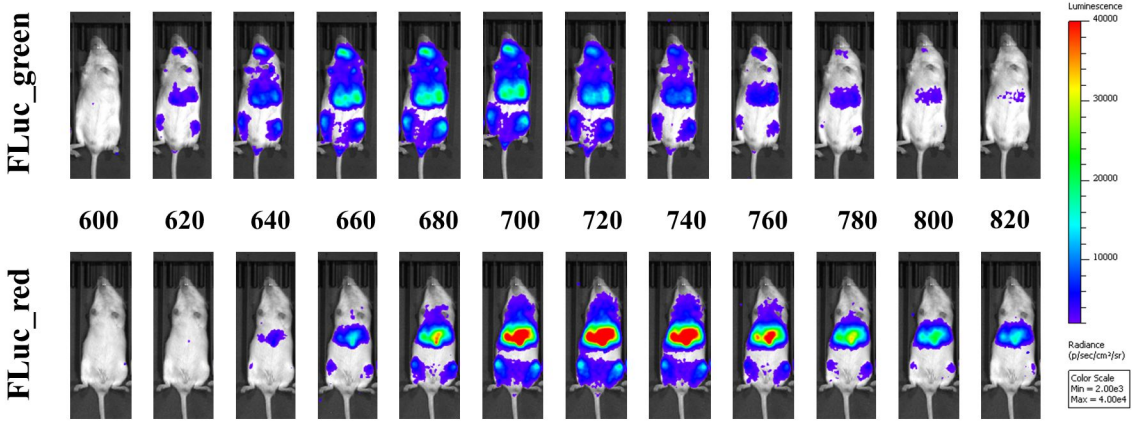

Intracranial

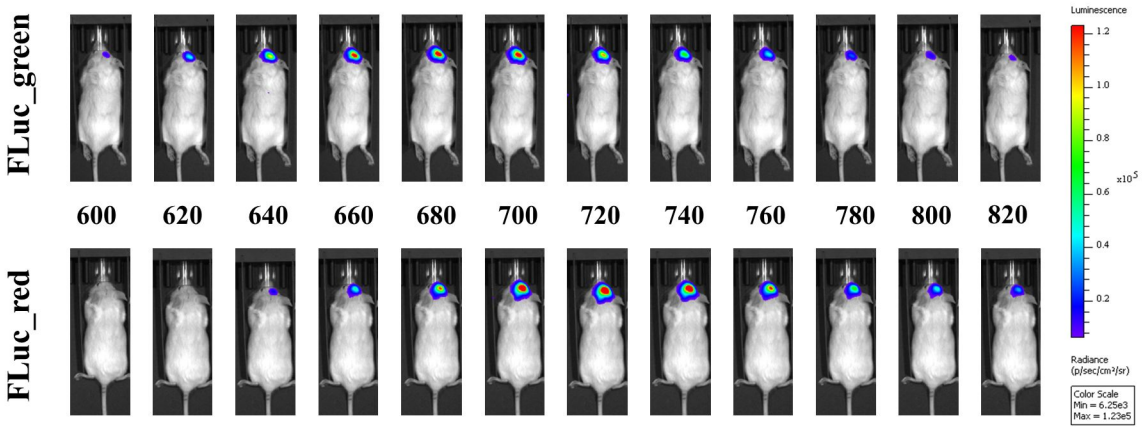

FIGURE 3 – FIGURE SUPPLEMENT 2

LH_2 FILTER IMAGES

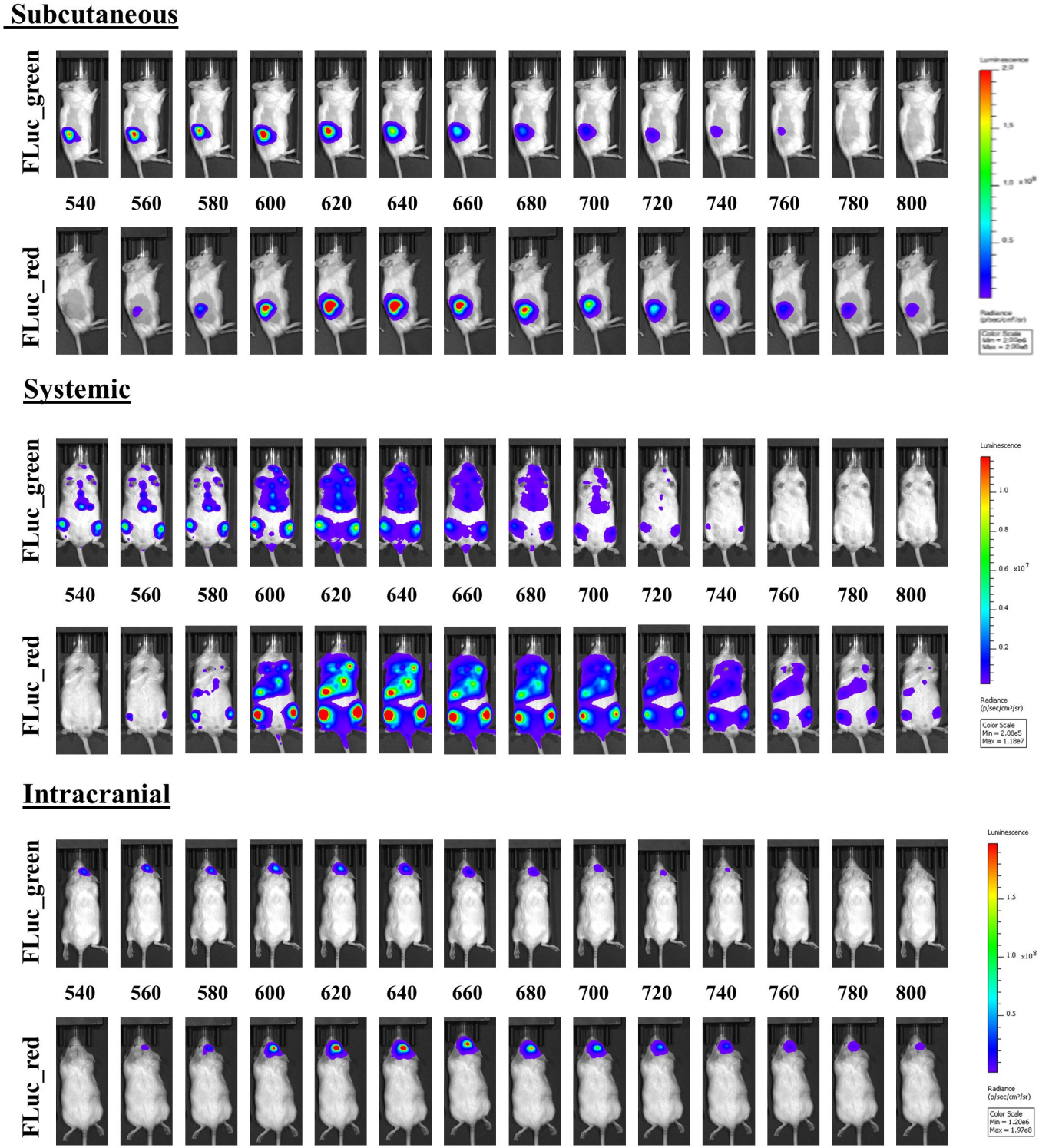

FIGURE 5 – FIGURE SUPPLEMENT 1